Why is HMBC superior to LR-HSQC? Influence of homonuclear couplings $J_{HH'}$ on the intensity of long-range correlations

Peter Bigler*, Julien Furrer*

Departement für Chemie und Biochemie, Universität Bern, Freiestrasse 3, CH-3012 Bern, Switzerland

***biglermeier@bluewin.ch (PB)**

***julien.furrer@dcb.unibe.ch (JF)**

Abstract Long-Range Heteronuclear Single Quantum Correlation (LR-HSQC) experiments may be applied as an alternative to Heteronuclear Multiple-Bond correlation **(**HMBC) experiments for detecting long-range correlations, but has never enjoyed popularity for that purpose. To the best of our knowledge, the exact reasons have not yet been fully established. For both experiments it is widely accepted that the evolution of proton-proton homonuclear couplings $J_{HH'}$ during the polarization transfer delays Δ leads to significant losses, and that the intensity of the observable coherence is zero when $J_{HH'}$ matches the condition $\Delta = 0.5/J_{HH'}$. Here, we analyze the influence of $J_{HH'}$ on the intensity of long-range correlations in HMBC and LR-HSQC spectra. We show that for both experiments long-range correlations *will not* be canceled because of homonuclear couplings $J_{HH'}$. Our theoretical and experimental results definitely establish and validate the superiority of HMBC-based experiments among the family of heteronuclear long-range correlation experiments: (i) the overall cross peak's intensity is higher, and (ii) in LR-HSQC experiments the intensity of the long-range cross peaks is additionally influenced in an unwanted way by the magnitude and number of passive homonuclear proton-proton couplings $J_{HH'}$.

Keywords: NMR, ^{1}H, ^{13}C, HMBC, LR-HSQC, homonuclear couplings, cross peak intensity, product operator.

This article has been accepted for publication and undergone full peer review but has not been through the copyediting, typesetting, pagination and proofreading process which may lead to differences between this version and the Version of Record. Please cite this article as doi: 10.1002/mrc.4762

This article is protected by copyright. All rights reserved.

Accepted Article

Introduction

Heteronuclear long-range correlation experiments correlate protons and heteronuclei exploiting $^{n}J_{HX}$ long-range couplings. The experiments are essential to connect structural fragments across non-protonated carbons or heteroatoms.[1-9] Prior to the introduction of proton-detected NMR methods, experiments such as long-range HETCOR and FLOCK were used for this purpose.[10] Currently, there are a plethora of proton-detected methods available for long-range heteronuclear shift correlation.[10-13] The oldest and still, probably, most widely used long-range heteronuclear shift correlation experiment is the basic HMBC experiment described in 1986 by Bax and Summers.[14] This pulse sequence employs only a few RF pulses, making it not only the most sensitive but also very robust in terms of RF inhomogeneity or poorly adjusted pulse lengths.[15] Despite its undeniable strengths, there are several important established issues associated with the basic HMBC experiment:[15, 16] (a) the detected proton magnetization is antiphase with respect to the active carbon which on the one hand prevents the use of carbon broadband decoupling during acquisition and which on the other hand may cancel the cross peaks due to unfavorable signal overlap with very small coupling constants;[17] (b) both multiple quantum coherences and homonuclear couplings ($J_{HH'}$) evolve during the entire t_1 evolution period, giving tilted and $J_{HH'}$-split multiplet structures along the F_1 dimension; and (c) the final signal intensity is proportional to $\sin(\pi^{n}J_{XH}\Delta)$ and depends – as outlined below – exclusively on the long-range heteronuclear coupling constant.

Several years after the introduction of the HMBC experiment, numerous variants were introduced. The addition of a delay Δ for refocusing heteronuclear couplings to the basic HMBC experiment has led to the D-HMBC,[18] which has never enjoyed the popularity of the basic HMBC experiment, although it generates in-phase $^{n}J_{XH}$ correlations and allows the application of ^{13}C decoupling during the acquisition time. During the period from 1998-2000, several “accordion” optimized long-range correlation experiments, aimed at equalizing the intensities of long-range correlations, were reported.[19-22] At the same time, the so-called constant-time (CT-) HMBC experiments with a t_1-evolution of fixed length were proposed.[23, 24] These experiments allow $J_{HH'}$ modulations in t_1 to be suppressed and provide cross peaks

This article is protected by copyright. All rights reserved.

Accepted Article

that are effectively decoupled in the indirect dimension with respect to $^{n}J_{HH'}$ (CT-HMBC-1) and to both $^{n}J_{XH}$ and $^{n}J_{HH'}$ (CT-HMBC-2), thus significantly improving the resolution and the sensitivity.[23]

In 2001, the sensitivity of the HMBC could be increased by as much as a factor of √2 compared with the basic HMBC experiment, by refocusing and detecting two orthogonal in-phase magnetization components.[25-27] This experiment is now known as SE-HMBC. The combination of CT-HMBC, SE-HMBC, an efficient low-pass *J* filter (for suppressing unwanted $^{1}J_{XH}$ artifacts),[28] and of the ASAP building block,[29] that significantly enhances the sensitivity and allows reducing the measurement time, has led to the IMPACT-HMBC experiment, which is probably the most useful and efficient sequence derived from the classical HMBC.[30] Most of these methods have been discussed in a number of reviews and the interested reader is referred to these for a more in-depth treatment of long-range heteronuclear correlation methods.[8, 15, 16, 31-33]

For all these HMBC variants, it was commonly pointed out that possible accidental cancellation of correlations may occur, because the amount of useful magnetization generated in the initial $^{n}J_{XH}$-evolution preparation period Δ is dependent not only on $^{n}J_{XH}$, but is additionally modulated by a trigonometric factor $\Sigma_i \cos(\pi J_{HHi}\Delta)$, due to the evolution of the homonuclear proton-proton J_{HHi} couplings.[15, 16, 31, 33] However, cross peaks in HMBC *always* and *exclusively* vanish when the long-range coupling evolution delay, Δ, matches the long-range heteronuclear coupling constant, $\Delta = k/^{n}J_{XH}$, as recently demonstrated by us.[34] The signal-to-noise ratio (SNR) of long-range correlations in HMBC spectra therefore *does not* depend upon the proton-proton homonuclear coupling.[34]

As an alternative to HMBC experiments long-range versions of HSQC[35-37] may be applied, but have obviously never enjoyed popularity for that purpose. Yet, HSQC-based techniques appear inherently more efficient, especially because the correlation peak shapes can be improved without a constant-time setting, as no $J_{HH'}$ modulation occurs during t_1. However, the $J_{HH'}$ evolution occurs during the long polarization transfer delays of the INEPT, and some of the magnetization will be transferred to homonuclear multiple-quantum coherence.[38, 39] Consequently the intensity of cross-peaks turns out to depend on both $^{n}J_{XH}$ and $^{n}J_{HH'}$ couplings. Therefore cross-peaks will not only be cancelled with $\Delta = k/^{n}J_{XH}$ but their intensity is

This article is protected by copyright. All rights reserved.

strongly and additionally influenced by the magnitude and number of passive homonuclear proton-proton $J_{HH'}$ couplings.

It is also commonly admitted that with HSQC the intensity of the observable $H_Y X_Z$ coherence (if a XHH' spin system is considered) is zero when $J_{HH'}$ matches the condition $\Delta = 0.5/J_{HH'}$.[39] We show however that long-range correlations will *not* be cancelled at this condition *and* generally do not cancel because of homonuclear couplings $J_{HH'}$. This is as outlined below because for e.g. a CHH' spin system, not only *one*, but *two* coherences which partially compensate each other actually contribute to the final signal.

As shown in this manuscript, HMBC-based experiments seem to perform better compared to long-range versions of HSQC, which clarifies why HSQCs have never enjoyed popularity for detecting long-range correlations. The main reason is however *not* that the observable long-range cross peaks is zero when $\Delta = 0.5/J_{HH'}$, but rather that the intensity of long-range correlations in HMBC spectra are by far less dependent on passive homonuclear proton-proton $J_{HH'}$ couplings, resulting in an improved visibility of cross-peaks and enhanced sensitivity in general compared to HSQC variants.

Results and Discussion

LR-HSQC experiment

Analysis for a CHH' spin system

We consider first the LR-HSQC experiment (Figure 1),[35, 36] also known under the acronym GSQMBC (Gradient-enhanced Single Quantum Multiple Bond Correlation) and initially designed for measuring small heteronuclear coupling constants, not accessible at that time with gradient-enhanced HMBC spectra[40] in magnitude mode presentation. In the following and throughout the manuscript, we'll only discuss CH_n spin systems, but the different conclusions can be generalized to other XH_n spin systems.

Accepted Article

This article is protected by copyright. All rights reserved.

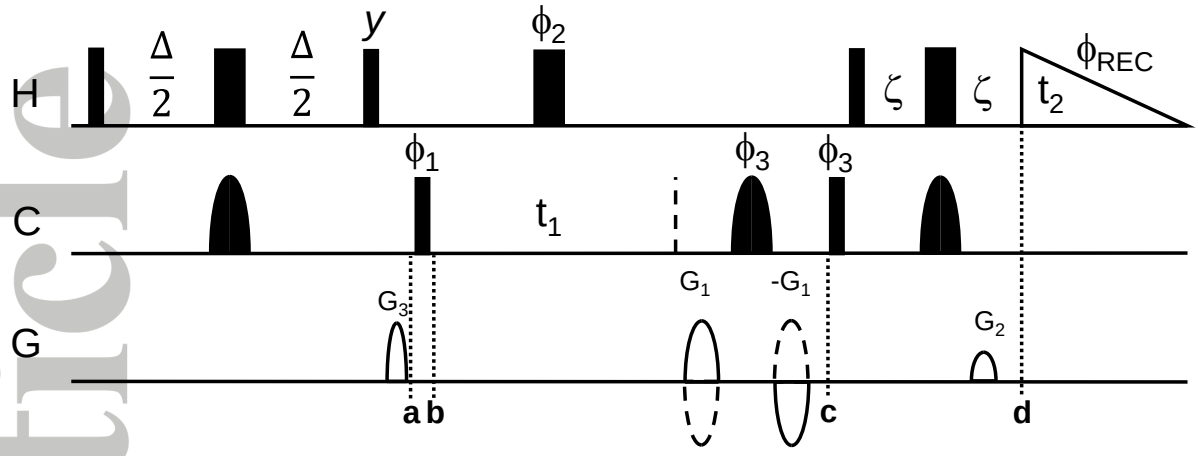

Figure 1. Pulse sequence of the LR-HSQC experiment with echo-antiecho gradient selection[36, 39] and without a low-pass filter (pulseprogram *hsqcetgplrsp* from the Bruker pulse sequence library). Thin bars represent 90° pulses, thick bars 180° pulses. The 180° pulses on the ^{13}C channel are advantageously replaced by broadband adiabatic inversion (first and third) and refocusing (second) pulses, shown as sine pulses. Δ is the long-range coupling evolution delay and is set to an average value $0.5/{}^{n}J_{CHav}$. Delay ζ is set to guarantee proper ^{1}H chemical shift refocusing and is equal to the length of G_2 + delay for gradient recovery. The following phase cycling is applied: ϕ_1 = *x, -x*; ϕ_2 = *x, x, -x, -x*; ϕ_3 = *4x, 4(-x)*; ϕ_{rec} = *x, -x, x, -x, -x, x, -x, x*. Phases not shown are applied along the *x*-axis. Gradient ratios: G_1:G_2:G_3= 40:20:34 (odd), -40:20:34 (even) for echo-/antiecho detection. The labels *a-d* denote the four steps of interest in the pulse sequence.

At point *a,* a product operator evaluation for a CHH' spin system, taking into account that all chemical shifts are refocused, yields the following coherences (H is a proton long-range coupled ($^{n}J_{CH}$) to carbon C and H' is a proton coupled to H through $J_{HH'}$, and considering $^{n}J_{CH}$ and $J_{HH'} \neq 0$). The subscript *r* will be used subsequently throughout the whole manuscript to emphasize that the proton H is long-range coupled to the carbon. Note that there is no difference if we consider $^{n}J_{CH'} \neq 0$. The reason is that both spins C and H' are present as *z*-magnetization during Δ, and therefore the *J*-coupling between them remains inactive.

$$H_Z^r \xrightarrow{(90)^\circ xH} -H_Y^r \xrightarrow{\pi\,{}^{n}J_{CH}\Delta 2H_Z C_Z} \xrightarrow{(180)^\circ xH} \xrightarrow{(180)^\circ xH'} \xrightarrow{(180)^\circ xC} \xrightarrow{(90)^\circ yH} \xrightarrow{(90)^\circ yH'}$$
$$- H_Y^r \cos(\pi J_{HH'}\Delta)\cos(\pi\,{}^{n}J_{CH}\Delta) - 2H_Z^r C_Z \cos(\pi J_{HH'}\Delta)\sin(\pi\,{}^{n}J_{CH}\Delta)$$
$$- 2H_Z^r H_X' \sin(\pi J_{HH'}\Delta)\cos(\pi\,{}^{n}J_{CH}\Delta) + 4H_Y^r H_X' C_Z \sin(\pi J_{HH'}\Delta)\sin(\pi\,{}^{n}J_{CH}\Delta) \quad (1)$$

This article is protected by copyright. All rights reserved.

The coherences present immediately after the second 90°$_y$ ^{1}H-pulse can be classified as follows: (i) a longitudinal coherence $2H^r_ZC_Z$, (ii) two pure proton single-quantum coherences H_Y and $2H^r_XH'_Z$ and (iii) a multi-quantum coherence $4H^r_YH'_XC_Z$. At this stage of the LR-HSQC sequence a spoil gradient G3 may be applied that dephases all but *z*-magnetizations and zero-quantum coherences.[41] Note that the pure proton coherences H^r_Y and $2H^r_XH'_Z$ can be ignored anyway, since on the one side they will not contribute to carbon coherence after the first 90° ^{13}C pulse for the subsequent ^{13}C-shift evolution period t_1, and on the other side they will be destroyed subsequently by the coherence selection gradients G1 and G2 (G1 = ±2, G2 = 1). It's worth to mention that with the Cartesian operators shown in equation 1, one might assume by mistake that only the longitudinal polarization $2H^r_ZC_Z$ (*z*-ordered state) survives after the spoil gradient G3. Therefore and to understand the effect of magnetic field gradients the Cartesian operators must be replaced by the respective raising and lowering operators. With the $4H^r_YH'_XC_Z$ coherence term correspondingly transformed it is obvious that it represents actually a sum of double (DQ) and zero (ZQ) quantum coherences:[42]

$$4H^r_YH'_XC_Z \;\rightarrow\; -i(H^r_+H'_+ + H^r_+H'_- - H^r_-H'_+ - H^r_-H'_-)C_Z$$
$$\qquad\qquad\quad DQ \qquad ZQ \qquad ZQ \qquad DQ$$

(2)

G3 turned off

The 90° pulse applied on the ^{13}C channel leads to:

$$\begin{aligned} &-2H^r_ZC_Z\cos(\pi J_{HH'}\Delta)\sin(\pi\,{}^nJ_{CH}\Delta) \quad -i(H^r_+H'_+ + H^r_+H'_- - H^r_-H'_+ \\ &\quad - H^r_-H'_-)C_Z\sin(\pi J_{HH'}\Delta)\sin(\pi\,{}^nJ_{CH}\Delta) \\ &\quad \xrightarrow{(90)^\circ xC} \quad -iH^r_Z(C_+ - C_-)\cos(\pi J_{HH'}\Delta)\sin(\pi\,{}^nJ_{CH}\Delta) \\ &\quad + 0.5(H^r_+H'_+ + H^r_+H'_- - H^r_-H'_+ - H^r_-H'_-)(C_+ - C_-)\sin(\pi J_{HH'}\Delta)\sin(\pi\,{}^nJ_{CH}\Delta) \end{aligned}$$

(3)

It can be seen that ^{13}C-single quantum coherences (SQ) and ^{1}H, ^{13}C-triple quantum coherences (TQ) are obtained:

This article is protected by copyright. All rights reserved.

$$-iH^r_Z C_+ + iH^r_Z C_-$$

SQ SQ

and

$$0.5(H^r_+H'_+C_+ + H^r_+H'_-C_+ - H^r_-H'_+C_+ - H^r_-H'_-C_+ - H^r_+H'_+C_- - H^r_+H'_-C_- + H^r_-H'_+C_- + H^r_-H'_-C_-)$$

TQ SQ SQ TQ TQ SQ SQ TQ

(4)

The various coherences correspond to different nuclei specific coherence levels CL_k e.g. $H^r_+H'_+C_+$ has coherence levels +2(^{1}H), +1(^{13}C) and $H^r_+H'_-C_+$ has coherence levels 0(^{1}H),+1(^{13}C).

In addition, not only the coherence levels but the corresponding resonance frequencies which in fact depend on the magnetogyric ratios of the involved nuclei have to be taken into account. Therefore and to obtain a detectable signal at the end of a selected coherence pathway, the following condition for the individual gradient strengths G_i and the correspondingly present (gyromagnetic-weighted) coherence levels CL_k across the pulse sequence must be fulfilled:[41]

$$\Sigma_i G_i \cdot CL_i \cdot \gamma_i = 0$$

Consequently, the triple quantum coherences $H^r_+H'_+C_+$, $H^r_-H'_-C_+$, $H^r_+H'_+C_-$, and $H^r_-H'_-C_-$ will be dephased by the subsequent coherence selection gradients G1 and G2 - with their strengths set to ratios 2:1 and -2:1 respectively - and can be ignored. The remaining ^{13}C-single quantum coherences, $iH^r_ZC_+$, $iH^r_ZC_-$, $H^r_+H'_-C_+$, $H^r_-H'_+C_+$, $H^r_+H'_-C_-$, and $H^r_-H'_+C_-$, on the other hand, will be finally rephased with these gradient settings and may be detected.

G3 turned on

The double-quantum terms of $4H^r_YH'_XC_Z$ in equation (2), $-i(H^r_+H'_+ - H^r_-H'_-)C_Z$ are dephased by the gradient G3 and can be ignored. The zero-quantum terms, $-i(H^r_+H'_- - H^r_-H'_+)C_Z$ – as well as the polarization $2H^r_ZC_Z$ - on the other hand, are left

This article is protected by copyright. All rights reserved.

Accepted Article

unaffected and continue to evolve. Therefore and including the $2H^r_ZC_Z$ term the 90° pulse applied on the ^{13}C channel leads to:

$$-2H^r_ZC_Z \rightarrow -iH^r_ZC_+ + iH^r_ZC_-$$

$$-i(H^r_+H'_- - H^r_-H'_+)C_Z \rightarrow 0.5(H^r_+H'_-C_+ - H^r_-H'_+C_+ - H^r_+H'_- C_- + H^r_-H'_+C_-)$$

(5)

which are ^{13}C-single quantum coherences that continue to evolve and will be selected with the strengths of the gradients G1 and G2 set to ratios 2:1 and -2:1 respectively. It is noteworthy that the outcome of the INEPT block is identical, irrespective of the purge gradient G3, which in fact is applied to ensure that no coherences will be present during the t_1-evolution period that did not take part in the INEPT transfer step.[43]

The coherences $-iH^rz(C_+ - C_-)$ evolve during the t_1 evolution period and the subsequent 180° ^{13}C-pulse as follows. Note that the two gradients G1 will select either the C_+ or the C_- coherence and that we keep only the coherences containing C_-):

$$iH^r_Z(C_- - C_+) \xrightarrow{t_1/2-(180)°xH^r,(180)°xH'-t_1/2-(180)°xC} \longrightarrow iH^r_ZC_- e^{i\pi\Omega_C t_1}$$

(6)

The coherences $0.5(H^r_+H'_-C_+ - H^r_-H'_+C_+ - H^r_+H'_-C_- + H^r_-H'_+C_-)$, which will be reduced by the two gradients G1 to $0.5(-H^r_+H'_- + H^r_-H'_+)C_-$ for the reasons mentioned above, evolve during the t_1 evolution period and the subsequent 180° ^{13}C-pulse as follows:

$$-0.5(H^r_+H'_- - H^r_-H'_+)C_- \xrightarrow{t_1/2-(180)°xH^r,(180)°xH'-t_1/2-(180)°xC} \longrightarrow 0.5(H^r_+H'_- - H^r_-H'_+)C_-e^{i\pi\Omega_C t_1}$$

(7)

The second pair of 90° pulses applied on both channels will convert the $H^r_ZC_-$ antiphase coherence into observable proton antiphase magnetization $H^r_-C_Z$ and will

This article is protected by copyright. All rights reserved.

convert the $H^r_+H'_-C_-$ and $H^r_-H'_+C_-$ coherences into observable proton antiphase magnetization $H^r_-H'_ZC_Z$ (the effects of the delays ζ and the second pair of simultaneous 180° ^{1}H and ^{13}C pulses are neglected):

$$iH^r_Z C_- \, e^{i\pi\Omega_C t_1} \xrightarrow{(90°)_x C} \xrightarrow{(90°)_x H^r} \xrightarrow{(90°)_x H'} -0.5iH^r_- C_Z \, e^{i\pi\Omega_C t_1} \quad (8)$$

$$0.5(H^r_+H'_- - H^r_-H'_+)C_- e^{i\pi\Omega_C t_1} \xrightarrow{(90°)_x C} \xrightarrow{(90°)_x H^r} \xrightarrow{(90°)_x H'} 0.5H^r_- H'_Z C_Z \, e^{i\pi\Omega_C t_1} \quad (9)$$

Thus, at *d*, before acquisition, we have (including the corresponding trigonometric factors):

$$-0.5iH^r_- C_Z \, e^{i\pi\Omega_C t_1} \cos(\pi J_{HH'}\Delta) \sin(\pi \, {}^n J_{CH}\Delta) + 0.5H^r_- H'_Z C_Z \, e^{i\pi\Omega_C t_1} \sin(\pi J_{HH'}\Delta) \sin(\pi \, {}^n J_{CH}\Delta) \quad (10)$$

The two coherences represent dispersive *y*-magnetization of spin H^r antiphase with respect to spin C and absorptive *x*-magnetization of spin H^r doubly antiphase with respect to spin H' and C. Importantly, the presence of cross-peaks with mixed phase can lead to the accidental signal cancellation, especially if the magnitudes of the different coupling constants $^nJ_{CH}$ and $J_{HH'}$ and the linewidths of the individual lines are of the same order. In this respect, the digital resolution in F2 is also important and recording the data with sufficient points is mandatory.[44]

It turns out that in LR-HSQC experiments long-range proton-carbon cross-peaks *do not* cancel when the homonuclear coupling $J_{HH'}$ accidentally matches multiples of twice the long-range coupling evolution delay Δ, i.e. when $\cos(\pi J_{HH'}\Delta) = 0$. To the best of our knowledge, this somewhat surprising characteristic has not been reported so far,[38, 39] but it appears absolutely consistent: According to equation (10) and since the $H^r_-C_Z$ shows a $\cos(\pi^n J_{HH'}\Delta)$- and the $H^r_-H'_ZC_Z$ a $\sin(\pi^n J_{HH'}\Delta)$-dependence at least one of the two $^nJ_{HH'}$-dependent coherence components will be >0 and obviously compensate in part each other when Δ is

This article is protected by copyright. All rights reserved.

Accepted Article

varied. Cancelation of long-range proton-carbon correlations in LR-HSQC spectra *only* occurs when the delay Δ unintentionally fulfills the condition $\Delta = k/{}^{n}J_{CH}$, k = 1, 2,..,. The effect of homonuclear coupling $J_{HH'}$ shows up as intermediate drops of the intensity and with a general decrease in sensitivity as corroborated by corresponding simulations (Figure 2).

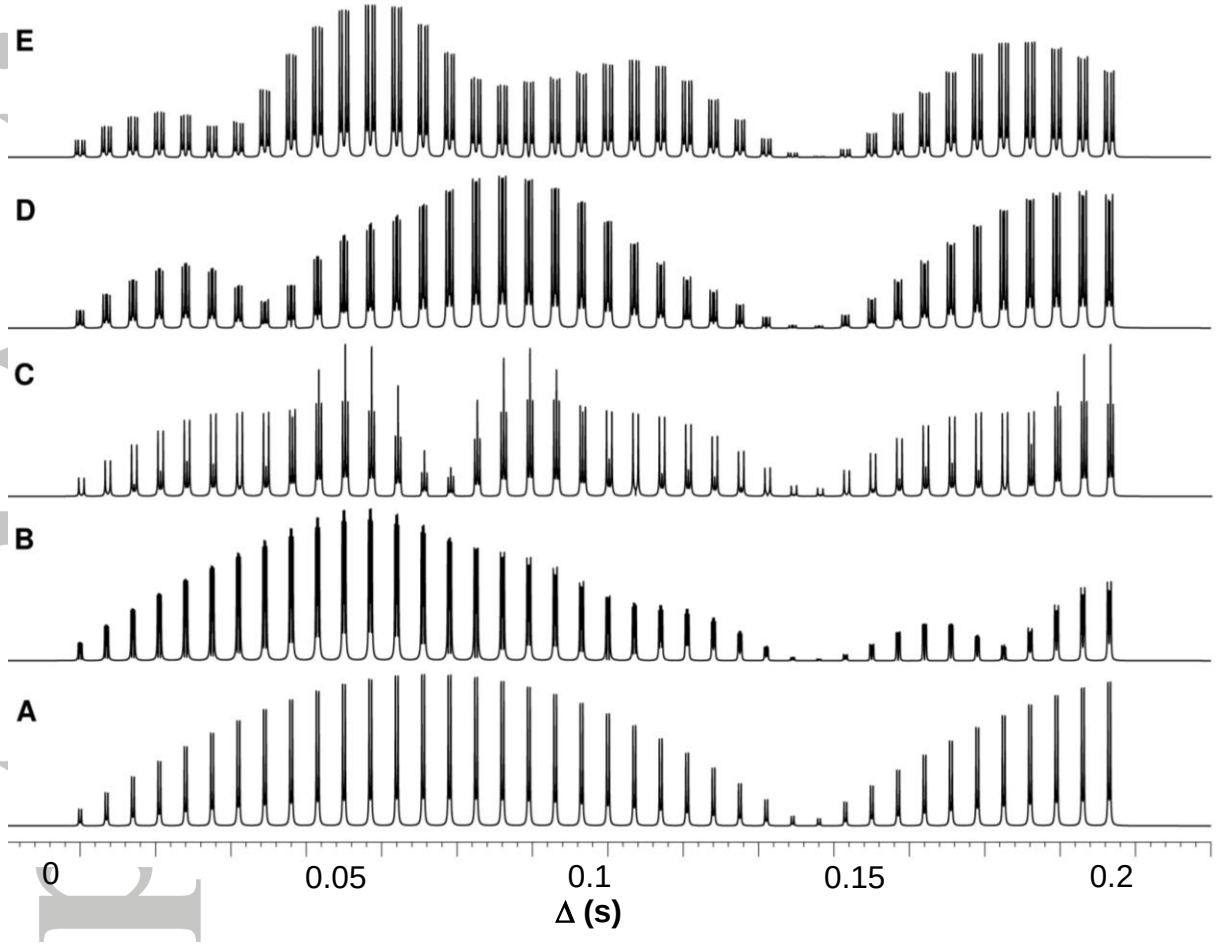

Figure 2. Simulated spectra obtained for a CHH' spin system, using the 1D ^{13}C selective version of the LR-HSQC pulse sequence shown in Figure 1 as a function of Δ. For better visualization the spectra are displayed in magnitude mode. (A) ${}^{n}J_{CH}$ = 7 Hz, $J_{HH'}$ = 0, (B) ${}^{n}J_{CH}$ = 7 Hz, $J_{HH'}$ = 3 Hz, (C) ${}^{n}J_{CH}$ = 7 Hz, $J_{HH'}$ = 7 Hz, (D) ${}^{n}J_{CH}$ = 7 Hz, $J_{HH'}$ = 11 Hz, (E) ${}^{n}J_{CH}$ = 7 Hz, $J_{HH'}$ = 17 Hz. Zero intensity in the simulated spectra occurs exclusively with $\Delta = 1/{}^{n}J_{CH}$. Simulations have been performed with the BRUKER NMRSIM program for MAC (version 5.5.3. 2012).

Yet, as demonstrated by Figure 2, homonuclear couplings $J_{HH'}$ will not additionally zero the peak's intensity when Δ is varied. However, and depending on the size $J_{HH'}$ of the homonuclear coupling signal intensities may be decreased to

This article is protected by copyright. All rights reserved.

such a degree that long-range proton-carbon cross peaks may be very weak or even absent.

Analysis for a CHH'H'' spin system

Similar calculations can be performed for a CHH'H'' spin system assuming ${}^{n}J_{CH}$, $J_{HH'}$, $J_{HH''} \neq 0$, ${}^{n}J_{CH'}$, ${}^{n}J_{CH''} = 0$. This system represents a usual AMQX spin system, where A = ^{1}H, M and Q = remote ^{1}H, and X = ^{13}C. At a, the following coherences are present (omitting the pure proton coherences that are subsequently dephased by the magnetic field gradients):

$$-2H^{r}_{Z}C_{Z}\cos(\pi J_{HH'}\Delta)\cos(\pi J_{HH''}\Delta)\sin(\pi J_{CH}\Delta)$$
$$+4H^{r}_{Y}H''_{X}C_{Z}\cos(\pi J_{HH'}\Delta)\sin(\pi J_{HH''}\Delta)\sin(\pi J_{CH}\Delta)$$
$$+4H^{r}_{Y}H'_{X}C_{Z}\sin(\pi J_{HH'}\Delta)\cos(\pi J_{HH''}\Delta)\sin(\pi J_{CH}\Delta)$$
$$+8H^{r}_{Z}H'_{X}H''_{X}C_{Z}\sin(\pi J_{HH'}\Delta)\sin(\pi J_{HH''}\Delta)\sin(\pi J_{CH}\Delta)$$
(11)

The last three terms can be rewritten again using the raising and lowering operators as:

$$4H^{r}_{Y}H'_{X}C_{Z} \rightarrow i(H^{r}_{+}H'_{+} + H^{r}_{+}H'_{-} - H^{r}_{-}H'_{+} - H^{r}_{-}H'_{-})C_{Z}$$
$$4H^{r}_{Y}H''_{X}C_{Z} \rightarrow i(H^{r}_{+}H''_{+} + H^{r}_{+}H''_{-} - H^{r}_{-}H''_{+} - H^{r}_{-}H''_{-})C_{Z}$$
$$8H^{r}_{Z}H'_{X}H''_{X}C_{Z} \rightarrow 2(H'_{+}H''_{+} + H'_{+}H''_{-} + H'_{-}H''_{+} + H'_{-}H''_{-})H^{r}_{Z}C_{Z}$$
(12)

As mentioned above, the respective double quantum components of $4H^{r}_{Y}H'_{X}C_{Z}$ ($i(H^{r}_{+}H'_{+} - H^{r}_{-}H'_{-})C_{Z}$), $4H^{r}_{Y}H''_{X}C_{Z}$ ($i(H^{r}_{+}H''_{+} - H^{r}_{-}H''_{-})C_{Z}$) and $8H^{r}_{Z}H'_{X}H''_{X}C_{Z}$ $(H'_{+}H''_{+} + H'_{-}H''_{-})H^{r}_{Z}C_{Z}$ are dephased by the gradient G3 and can be ignored. The respective zero quantum components, $(i(H^{r}_{+}H'_{-} - H^{r}_{-}H'_{+})C_{Z})$, $(i(H^{r}_{+}H''_{-} - H^{r}_{-}H''_{+})C_{Z})$ and $2(H'_{+}H''_{-} + H'_{-}H''_{+})H^{r}_{Z}C_{Z}$, on the other hand, together with the $2H^{r}_{Z}C_{Z}$ term, are left unaffected by G3, continue to evolve and are retained respectively.

This article is protected by copyright. All rights reserved.

Accepted Article

The 90° pulse applied on the ^{13}C channel leads to the following coherences (the trigonometric factors are omitted for clarity). Note that – for final detection of the wanted ^{1}H signal - the gradients G1 and G2 (with their strengths set to ratios 2:1 and -2:1) will select C_+ or C_- respectively. For clarity only the C_+ terms are listed:

$$-iH^r_ZC_+$$
$$-0.5(H^r_+H'_-C_+ - H^r_-H'_+C_+)$$
$$-0.5(H^r_+H''_-C_+ - H^r_-H''_+C_+)$$
$$i(H'_+H''_-C_+ + H'_-H''_+C_+)H^r_Z$$

(13)

After the t_1 evolution time and the subsequent 180° ^{13}C-pulse the second pair of 90° pulses applied on both channels converts these coherences into observable proton antiphase magnetization H_-C_Z, $H_-H'_ZC_Z$, $H_-H''_ZC_Z$ and $H_-H'_ZH''_ZC_Z$ (the effects of the delays ζ and of the second pair of simultaneous 180° ^{1}H and ^{13}C pulses are neglected).

$$-iH^r_Z\,C_+ \xrightarrow{t_1/2-(180)^\circ xH^r,(180)^\circ xH'-t_1/2-\ (180)^\circ xC\ \ (90)^\circ xC\ (90)^\circ yH^r\ (90)^\circ yH'} -0.5H^r_-C_Ze^{i\pi\Omega_Ct_1}$$

$$-0.5(H^r_+H'_-C_+ - H^r_-H'_+C_+) \xrightarrow{t_1/2-(180)^\circ xH^r,(180)^\circ xH'-t_1/2-\ (180)^\circ xC\ \ (90)^\circ xC\ (90)^\circ yH^r\ (90)^\circ yH'} -0.5iH^r_-C_ZH'_Ze^{i\pi\Omega_Ct_1}$$

$$-0.5(H^r_+H''_-C_+ - H^r_-H''_+C_+) \xrightarrow{t_1/2-(180)^\circ xH^r,(180)^\circ xH''-t_1/2-\ (180)^\circ xC\ \ (90)^\circ xC\ (90)^\circ yH^r\ (90)^\circ yH''} -0.5iH^r_-C_ZH''_Ze^{i\pi\Omega_Ct_1}$$

$$i(H'_+H''_-C_+ + H'_-H''_+C_+)H^r_Z \xrightarrow{t_1/2-(180)^\circ xH^r,(180)^\circ xH',(180)^\circ xH''-t_1/2-\ (180)^\circ xC\ \ (90)^\circ xC\ (90)^\circ yH^r\ (90)^\circ yH'\ (90)^\circ yH''} H^r_-H'_ZH''_ZC_Ze^{i\pi\Omega_Ct_1}$$

+ non-observable multiple-quantum coherences

(14) (f_A-f_D)

The term $H^r_-C_Z$ (f_A) represents *x*-magnetization of spin H antiphase with respect to spin C, the term $iH^r_-H'_ZC_Z$ (f_B) represents *y*-magnetization of spin H which is doubly

This article is protected by copyright. All rights reserved.

antiphase with respect to spin C and spin H', the term $iH^{r}\text{-}H''_{Z}C_{Z}$ (f_C) represents *y*-magnetization of spin H which is doubly antiphase with respect to spin C and spin H'', and the term $H^{r}\text{-}H'_{Z}H''_{Z}C_{Z}$ (f_D) represents *x*-magnetization of spin H which is triply antiphase with respect to spin C and spins H' and H''. Thus, the magnitude of all four terms not only depends on the evolution of the $^{n}J_{CH}$ coupling, but also on the evolution of the homonuclear $J_{HH'}$ and $J_{HH''}$ couplings.

As for a CHH' spin system, additional zeroing of signal intensities caused by $J_{HH'}$ and $J_{HH''}$ does not occur and the accidental cancelation of the long-range proton-carbon correlations due to homonuclear couplings $J_{HH'}$ and $J_{HH''}$ does not exist. Homonuclear coupling however causes several Δ–dependent drops of the intensity accompanied with a general decrease in sensitivity (Figure S2).

Finally, we wish to mention that several versions of the LR-HSQC have been reported to minimize $J_{HH'}$ evolution by adding CPMG elements during the INEPT block (CPMG-INEPT), for the observation of exchange broadened signals in proteins,[45] and to improve the quantitative measurement of long-range coupling constants $^{n}J_{CH}$ from complex multiplets patterns.[39, 46, 47] It would be interesting to compare the LR-CAHSQC[39] or CPMG-HSQMBC[46] experiments with the HMBC in terms of sensitivity/number of cross peaks.

HMBC experiment

Analysis for a CHH' spin system

Compared to the LR-HSQC experiment the outcome for the HMBC-SE pulse sequence[26] (Figure 3) is quite different. The reason is that now at a, before the t_1 evolution period, exclusively zero- and double quantum rather than single quantum coherence terms are present, which changes the spin dynamics in the remaining part of the sequence.

Accepted Article

This article is protected by copyright. All rights reserved.

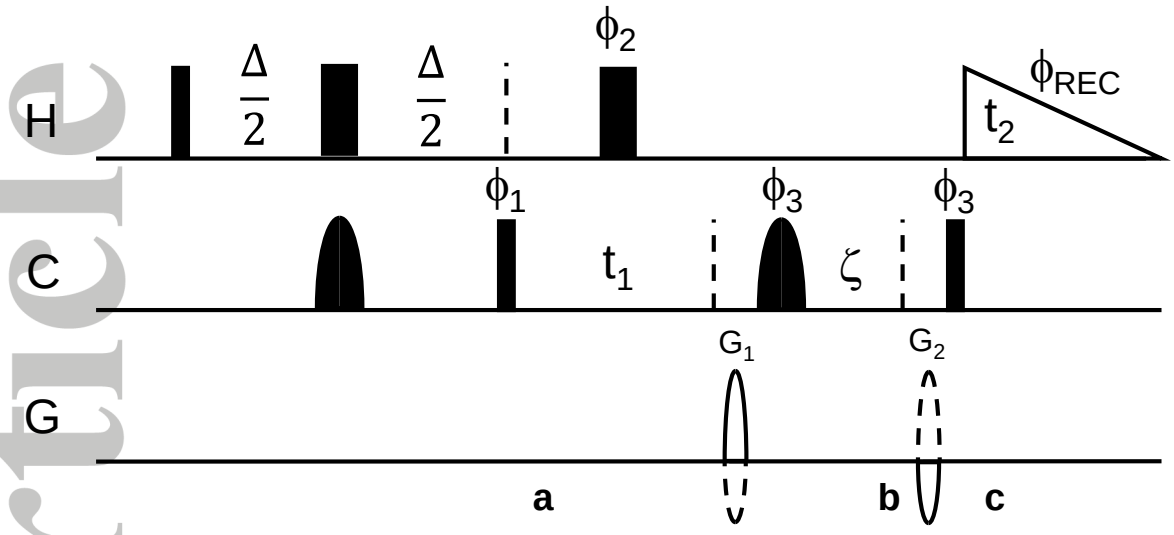

Figure 3. Pulse sequence of the slightly modified HMBC-SE experiment with echo-antiecho gradient selection[26, 27] and without low-pass *J* filter,[28] derived from the pulseprogram *hmbcetgpnd* of the Bruker pulseprogram library. Thin bars represent 90° pulses, thick bars 180° pulses. The 180° pulses on the ^{13}C channel are broadband adiabatic inversion (first) and refocusing (second) pulses, shown as sine pulses. Δ is the long-range coupling evolution delay and is set to an average value $0.5/^{n}J_{CHAv}$. Delay ζ is set to guarantee no ^{13}C chemical shift evolution for the first t_1 value, $\zeta = (t_1)_0 + p_{180H}$, where $(t_1)_0$ is the initial value of t_1, and p_{180H} is the duration of the proton 180° pulse. The following phase cycling is applied: ϕ_1 = *x, -x*; ϕ_2 = *x, x, -x, -x*; ϕ_3 = *4x, 4(-x)*; ϕ_{rec} = *x, -x, x, -x, -x, x, -x, x*. Pulses with no phase indicated are applied along the *x*-axis. Gradient ratios: G_1:G_2 = 50:-30 (odd), -30:50 (even) for echo-/antiecho detection. The labels *a-c* denote the three points of interest in the pulse sequence.

At point *a,* taking into account that all chemical shifts are refocused, a product operator evaluation for a CHH' spin system ($^{n}J_{CH}$, and $J_{HH'} \neq 0$, $^{n}J_{CH'} = 0$) shows that the following coherences are present:

$$H_Z^r \xrightarrow{(90°)_X H} -H_Y^r \xrightarrow{\pi\, {}^{n}J_{CH}\, \Delta 2H_Z C_Z} \xrightarrow{(180°)_X H} \xrightarrow{(180°)_X H'} \xrightarrow{(180°)_X C} \xrightarrow{\pi J_{HH'} \Delta 2H_Z H'_Z} \xrightarrow{(90°)_X C}$$

$$H_Y^r \cos(\pi J_{HH'}\Delta)\cos(\pi\, {}^{n}J_{CH}\Delta) + 2H_X^r C_Y \cos(\pi J_{HH'}\Delta)\sin(\pi\, {}^{n}J_{CH}\Delta)$$
$$- 2H_X^r H_Z^{'} \sin(\pi J_{HH'}\Delta)\cos(\pi\, {}^{n}J_{CH}\Delta) + 4H_Y^r H_Z^{'} C_Y \sin(\pi J_{HH'}\Delta)\sin(\pi\, {}^{n}J_{CH}\Delta)$$

(15)

This article is protected by copyright. All rights reserved.

As emphasized before for the LR-HSQC experiment, the pure proton coherences H^r_Y and $2H^r_XH'_Z$ will be dephased by the gradients G1 and G2 and can be ignored for the subsequent analysis. The term $2H^r_XC_Y$ (a superposition of double- and zero-quantum coherences, sometimes erroneously assumed to be the only term responsible for the desired HMBC correlation), and $4H^r_YH'_ZC_Y$ (also a superposition of double- and zero-quantum coherences which is antiphase with respect to spin H'), continue to evolve. In the following, for comparison with the LR-HSQC experiment and for understanding the effect of magnetic field gradients, we'll use again the respective raising and lowering operators.

$$2H^r_XC_Y \rightarrow -0.5i(H^r_+C_+ - H^r_+C_- + H^r_-C_+ - H^r_-C_-)$$
$$-4H^r_YH'_ZC_Y \rightarrow (-H^r_+C_+ + H^r_+C_- + H^r_-C_+ - H^r_-C_-)H'_Z \quad (16)$$

Note that in contrast to the LR-HSQC pulse sequence *both* double-quantum and zero-quantum components of the $2H^r_XC_Y$ and $4H^r_YH'_ZC_Y$ terms evolve in the subsequent t_1-evolution period. For clarity, we consider the evolution of both terms $-0.5i(H^r_+C_+ - H^r_+C_- + H^r_-C_+ - H^r_-C_-)$ and $(-H^r_+C_+ + H^r_+C_- + H^r_-C_+ - H^r_-C_-)H'_Z$ separately:

$-0.5i(H_+C_+ - H_+C_- + H_-C_+ - H_-C_-)$

The evolution of $-0.5i(H^r_+C_+ - H^r_+C_- + H^r_-C_+ - H^r_-C_-)$ during the t_1 evolution period and the subsequent 180° ^{13}C pulse provides (the effect of $J_{HH'}$ during t_1 is neglected, and the trigonometric factors are omitted for clarity) the following terms. Note that with final quadrature detection of e.g. H^r_- only the terms $H^r_-C_+$ and $H^r_-C_-$ are relevant.

$$-0.5i(H^r_-C_+ - H^r_-C_-) \xrightarrow{t_1/2-(180)^\circ xH^r,(180)^\circ xH'-t_1/2-(180)^\circ xC} -0.5i(H^r_-C_+ - H^r_-C_-)e^{i\pi\Omega_C t_1} \quad (17)$$

The final 90° ^{13}C pulse provides observable proton antiphase magnetization $H^r_-C_z$. Note that with the two ratios of the gradient strengths for G1 and G2 set to 5:-3 (and taking into account the 180° ^{13}C pulse) either the first or the second of these two terms will be transformed (and rephased) to a detectable proton signal

This article is protected by copyright. All rights reserved.

respectively and that these two, subsequently acquired proton signals are finally combined allowing for quadrature detection in t_1.

At *c* we have therefore:

$$-0.5i(H_-^r C_+ - H_-^r C_-)e^{i\pi\Omega_C t_1} \xrightarrow{(90)^\circ xC} 0.5H_-^r C_Z e^{i\pi\Omega_C t_1} + \text{non-observable DQ coherences} \quad (18)$$

(-H$_+$C$_+$ + H$_+$C$_-$ + H$_-$C$_+$ - H$_-$C$_-$)H'$_Z$

The evolution of *(-H$^r_+$C$_+$ + H$^r_+$C$_-$ + H$^r_-$C$_+$ - H$^r_-$C$_-$)H'$_Z$* during the t_1 evolution period provides (the effect of $J_{HH'}$ during t_1 is neglected, the trigonometric factors are omitted and only the terms $H^r_-C_+$ and $H^r_-C_-$ are relevant):

$$(H_-^r C_+ - H_-^r C_-)H_Z' \xrightarrow{t_1/2-(180)^\circ xH^r,(180)^\circ xH'-t_1/2-} \xrightarrow{(180)^\circ xC} (H_-^r C_+ - H_-^r C_-)H_Z' e^{i\pi\Omega_C t_1} \quad (19)$$

The 90° pulse applied on the ^{13}C channel provides observable proton antiphase magnetization *H^r-H'$_Z$C$_Z$*. At *c* we have:

$$(H_-^r C_+ - H_-^r C_-)H_Z' e^{i\pi\Omega_C t_1} \xrightarrow{(90)^\circ xC} iH_-^r C_Z H_Z' e^{i\pi\Omega_C t_1} + \text{non-observable DQ coherences} \quad (20)$$

Thus, before acquisition, including the trigonometric factors and with the results obtained for the two terms *2H^r_XC$_Y$* and *4H^r_YH'$_Z$C$_Y$* we have:

$$0.5H_-^r C_Z e^{i\pi\Omega_C t_1} \cos(\pi J_{HH'}\Delta)\sin(\pi\, {}^nJ_{CH}\Delta) + iH_-^r C_Z H_Z' e^{i\pi\Omega_C t_1} \sin(\pi J_{HH'}\Delta)\sin(\pi\, {}^nJ_{CH}\Delta) \quad (21)$$

(f_A) *(f_B)*

Accepted Article

This article is protected by copyright. All rights reserved.

The term $0.5H^r\text{-}C_z$ *(f_A)* represents *x*-magnetization of spin H^r antiphase with respect to spin C, and the term $iH^r\text{-}H'_ZC_z$ *(f_B)* represents *y*-magnetization of spin H^r which is doubly antiphase with respect to spin C and spin H'.

Note that for F1-band selective HMBC experiments,[24] t_1 cannot be considered as short compared to the homonuclear proton-proton coupling constants $J_{HH'}$. In this case, before acquisition, we obtain:

$$-0.5H^r_{-}C_Z e^{i\pi\Omega_C t_1}\cos(\pi J_{HH'}(\Delta+t_1))\sin(\pi\,{}^nJ_{CH}\Delta) + iH^r_{-}C_Z H'_Z e^{i\pi\Omega_C t_1}\sin(\pi J_{HH'}(\Delta+t_1))\sin(\pi\,{}^nJ_{CH}\Delta)$$

The final signal intensity depends therefore upon Δ for the heteronuclear coupling ${}^nJ_{CH}$ but upon $\Delta + t_1$ for the homonuclear coupling $J_{HH'}$. Nevertheless, the length of t_1 has *no* influence on the intensity of the cross peak, as shown by us[34] and summarized below.

The final expression for the final signal S_M using a magnitude mode processing can be written as:[34]

$$S_M \sim \sin(\pi {}^nJ_{CH}\Delta)\times A_M = \sin(\pi {}^nJ_{CH}\Delta)\times B_M \quad (22)$$

where $A_M = (A_{R(abs)} + A_{I(disp)})^{0.5}$ and $B_M = (B_{R(abs)} + B_{I(disp)})^{0.5}$, $A_{R(abs)}$ and $B_{R(abs)}$ being the absorptive multiplet lines throughout as the real part and $A_{I(disp)}$ and $B_{I(disp)}$ the dispersive multiplet lines throughout as the imaginary part.

Equation 22 demonstrates that there is absolutely no $J_{HH'}$ dependent influence of the initial Δ delay on the cross-peak intensity (Figure 4). Note also that the evolution of homonuclear couplings $J_{HH'}$ during t_1 do not affect cross-peak intensities but are only responsible for corresponding signal modulations in t_1 (and corresponding splitting in F_1). Cross-peak intensities may however be reduced by short T_2 relaxation times.

For the special case where $J_{HH'} = {}^nJ_{CH}$, $A_M \neq B_M$, with an overlap of the center lines (Figure 4) the final signal S_M using a magnitude mode processing can be written as:[34]

This article is protected by copyright. All rights reserved.

$$S_M \sim \sin(\pi {}^nJ_{CH}\Delta)\times\left[\cos^2(\pi J_{HH'}\Delta)\times A_M^2+\sin^2(\pi J_{HH'}\Delta)\times B_M^2\right]^{1/2} \quad (23)$$

In this case, but also with ${}^nJ_{CH} \approx {}^nJ_{HH'}$ the intensities of the individual multiplet lines no longer behave uniformly but are influenced by ${}^nJ_{HH'}$. However and most importantly, the intensities of all multiplet lines still follow the uniform sine dependence imposed by the long range heteronuclear ${}^nJ_{CH}$ coupling constant (Figure 4c).

In summary and as corroborated by equation (22) the intensity of an HMBC cross peak for a H^{r}H'C-three-spin system *never* vanishes because of an accidental $\Delta/J_{HH'}$, combination, but *only* when the long-range evolution delay Δ equals a multiple of the inverse of the heteronuclear coupling constant ${}^nJ_{CH}$ (Figure 4).

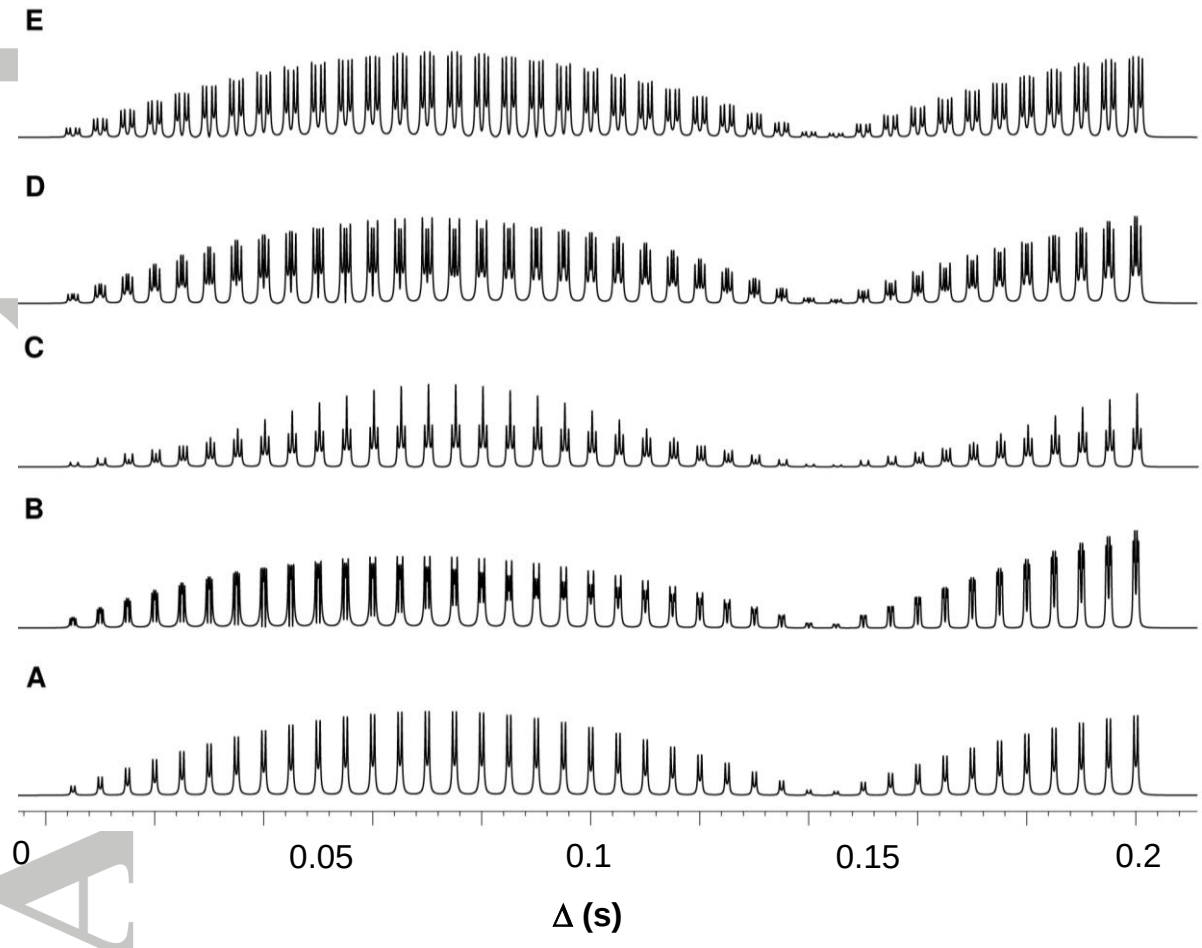

Figure 4. Simulated spectra obtained for a CHH' spin system, using the 1D version of the HMBC-SE pulse sequence shown in Figure 3 as a function of Δ. For clarity the

This article is protected by copyright. All rights reserved.

spectra are displayed in magnitude mode. (A) $^{n}J_{CH}$ = 7 Hz, $J_{HH'}$ = 0, (B) $^{n}J_{CH}$ = 7 Hz, $J_{HH'}$ = 3 Hz, (C) $^{n}J_{CH}$ = 7 Hz, $J_{HH'}$ = 7 Hz, (D) $^{n}J_{CH}$ = 7 Hz, $J_{HH'}$ = 11 Hz, (E) $^{n}J_{CH}$ = 7 Hz, $J_{HH'}$ = 17 Hz. The intensity-zeroes in the simulated spectra occur when Δ matches the conditions $\Delta = k/^{n}J_{CH}$, k = 0, 1, 2,.., n. Simulations have been performed with the BRUKER NMRSIM program for MAC (version 5.5.3. 2012).

It's useful to compare the observable coherences present before acquisition in both the LR-HSQC and HMBC experiments. For the LR-HSQC experiment, we have (Equation 10):

$$-0.5iH_{-}^{r}C_{Z}\, e^{i\pi\Omega_{C}t_{1}} \cos(\pi J_{HH'}\Delta) \sin(\pi\, ^{n}J_{CH}\Delta) + 0.5H_{-}^{r}H_{Z}'C_{Z}\, e^{i\pi\Omega_{C}t_{1}} \sin(\pi J_{HH'}\Delta) \sin(\pi\, ^{n}J_{CH}\Delta)$$

And for the HMBC experiment (Equation 21):

$$0.5H_{-}^{r}C_{Z}e^{i\pi\Omega_{C}t_{1}} \cos(\pi J_{HH'}\Delta) \sin(\pi\, ^{n}J_{CH}\Delta) + iH_{-}^{r}H_{Z}'C_{Z}e^{i\pi\Omega_{C}t_{1}} \sin(\pi J_{HH'}\Delta) \sin(\pi\, ^{n}J_{CH}\Delta)$$

Both coherences are identically composed of the same terms, except that they 90° out of phase and especially that the doubly antiphase magnetization is twice as intense in the case of the HMBC. This reflects the fact that in the LR-HSQC experiment, the double-quantum part of $4H^{r}_{Y}H'_{X}C_{Z}$, $i(H^{r}_{+}H'_{+} - H^{r}_{-}H'_{-})Cz$, is eliminated after the INEPT transfer period, and only the zero-quantum part $i(H^{r}_{+}H'_{-} - H^{r}_{-}H'_{+})Cz$ contributes to the final signal, while in the HMBC experiment, *both* the double-quantum and zero-quantum parts $(-H^{r}_{+}C_{+} + H^{r}_{+}C_{-} + H^{r}_{-}C_{+} - H^{r}_{-}C_{-})H'_{Z}$ survive and contribute to the final signal (Figure S4). In other words the $J_{HH'}$ and Δ dependent intensity variations of the two terms $H^{r}_{-}C_{Z}$ and $H^{r}_{-}H'_{Z}C_{Z}$ on $J_{HH'}$ for the initial Δ delay compensate each other ideally in the HMBC experiment, but only partially in the LR-HSQC experiment. Consequently cross-peak intensities are governed *solely* by $^{n}J_{CH}$ with the HMBC experiment, but are additionally influenced by $J_{HH'}$ with the LR-HSQC experiment. This gives rise to additional Δ dependent intensity drops and a general decrease in sensitivity for the latter (Figure S4).

Another aspect that might influence the final cross peak's intensity is the potential different relaxation behavior of the magnetization terms present in both experiments. In the LR-HSQC experiment, SQ relaxation effects are relevant, while in the HMBC, DQ and ZQ effects are applicable. As such, the HMBC experiment

This article is protected by copyright. All rights reserved.

Accepted Article

would likely be slightly more sensitive for proton deficient molecules (requiring long Δ values) with typically shorter relaxation times.[48]

Analysis for a CHH'H'' spin system

We can consider the situation of CHH'H'' spin system, with ${}^{n}J_{CH}$, $J_{HH'}$, $J_{HH''} \neq 0$, ${}^{n}J_{CH'}$, ${}^{n}J_{CH''} = 0$. The analysis for such a spin system is very lengthy, and therefore only some intermediate and the final results will be given. At a, four operators are present:

$$
\begin{aligned}
&-2H_X^r C_Y \cos(\pi J_{HH'}\Delta)\cos(\pi J_{HH''}\Delta)\sin(\pi {}^{n}J_{CH}\Delta)\\
&-4H_Y^r H_Z^{''} C_Y \cos(\pi J_{HH'}\Delta)\sin(\pi J_{HH''}\Delta)\sin(\pi {}^{n}J_{CH}\Delta)\\
&-4H_Y^r H_Z^{'} C_Y \sin(\pi J_{HH'}\Delta)\cos(\pi J_{HH''}\Delta)\sin(\pi {}^{n}J_{CH}\Delta)\\
&+8H_X^r H_Z^{'} H_Z^{''} C_Y \sin(\pi J_{HH'}\Delta)\sin(\pi J_{HH''}\Delta)\sin(\pi {}^{n}J_{CH}\Delta)
\end{aligned}
$$

(24)

They can be rewritten using the raising and lowering operators as (omitting the trigonometric factors for simplicity):

$$
\begin{aligned}
-2H^r_X C_Y &\rightarrow 0.5i(H_+C_+ - H_+C_- + H_-C_+ - H_-C_-)\\
-4H_Y H'_Z C_Y &\rightarrow (H_+C_+ - H_+C_- - H_-C_+ + H_-C_-)H'_Z\\
-4H_Y H''_Z C_Y &\rightarrow (H_+C_+ - H_+C_- - H_-C_+ + H_-C_-)H''_Z\\
8H^r_X H'_Z H''_Z C_Y &\rightarrow -2i(H_+C_+ - H_+C_- + H_-C_+ - H_-C_-)H'_Z H''_Z
\end{aligned}
$$

(25)

Assuming again that the evolution time t_1 is short compared to the homonuclear couplings $J_{HH'}$, i.e. neglecting modulations due to homonuclear couplings in t_1, we obtain at c (the trigonometric factors are omitted for clarity and only the final coherences containing H- are shown):

$$
0.5i(H_+^r C_+ - H_+^r C_- + H_-^r C_+ - H_-^r C_-)
\xrightarrow{t_1/2-(180)^\circ x H^r,(180)^\circ x H' - t_1/2-} \xrightarrow{(180)^\circ x C} \xrightarrow{(90)^\circ x C} 0.5H_-^r C_Z e^{i\pi\Omega_C t_1}
$$

This article is protected by copyright. All rights reserved.

$$(H_+^r C_+ - H_+^r C_- - H_-^r C_+ + H_-^r C_-)H'_Z$$
$$\xrightarrow{t_1/2-(180)°xH^r,(180)°xH'-t_1/2-} \xrightarrow{(180)°xC} \xrightarrow{(90)°xC} iH_-^r H'_Z C_Z e^{i\pi\Omega_C t_1}$$

$$(H_+^r C_+ - H_+^r C_- - H_-^r C_+ + H_-^r C_-)H''_Z$$
$$\xrightarrow{t_1/2-(180)°xH^r,(180)°xH'-t_1/2-} \xrightarrow{(180)°xC} \xrightarrow{(90)°xC} iH_-^r H''_Z C_Z e^{i\pi\Omega_C t_1}$$

$$-2i(H_+^r C_+ - H_+^r C_- + H_-^r C_+ - H_-^r C_-)H'_Z H''_Z \xrightarrow{t_1/2-(180)°xH^r,(180)°xH'-t_1/2-} \xrightarrow{(180)°xC} \xrightarrow{(90)°xC}$$
$$-2H_-^r H'_Z H''_Z C_Z e^{i\pi\Omega_C t_1}$$

+ non-observable multiple-quantum coherences

(26) (f_A-f_D)

Note that only these four terms are present and detected, even if *all* $J_{HH'} \neq 0$, but also if the carbon is coupled not only to H but for instance also to H'.

The four terms, but not their intensities (see below), are identical to those obtained for the LR-HSQC experiment: *x*-magnetization of spin H antiphase with respect to spin C, H^r-C_Z (f_A) represents, *y*-magnetization of spin H doubly antiphase with respect to spin C and spin H', iH^r-H'_ZC_Z (f_B), *y*-magnetization of spin H which is doubly antiphase with respect to spin C and spin H'', iH^r-H''_ZC_Z (f_C), and *x*-magnetization of spin H which is triply antiphase with respect to spin C and spins H' and H'', H^r-$H'_ZH''_ZC_Z$ (f_D).

Again as aforementioned, the final signal of the magnetization present before acquisition will therefore be calculated as the sums S_R and S_I of all absorptive and dispersive components, and with the two sums the signal intensity will be calculated in magnitude mode. It turns out that, also for a CHH'H'' spin system, the intensity of an HMBC cross peak *never* vanishes because of an accidental $\Delta/J_{HH'}$ combination, but *only* when the long-range evolution delay Δ equals the inverse of the heteronuclear coupling constant $^nJ_{CH}$ (Figure S5).

If the terms present before acquisition in both the LR-HSQC and HMBC experiments are compared (Equations 14&26), it can be seen that the doubly and triply antiphase coherences are twice as intense in the case of the HMBC (Figure S6).

This article is protected by copyright. All rights reserved.

Accepted Article

LR-HSQC:

$$-0.5H_-^r C_Z e^{i\pi\Omega_C t_1}\cos(\pi J_{HH'}\Delta)\cos(\pi J_{HH''}\Delta)\sin(\pi\,{}^nJ_{CH}\Delta)$$
$$-0.5iH_-^r H_Z' C_Z e^{i\pi\Omega_C t_1}\cos(\pi J_{HH'}\Delta)\sin(\pi J_{HH''}\Delta)\sin(\pi\,{}^nJ_{CH}\Delta)$$
$$-0.5iH_-^r H_Z'' C_Z e^{i\pi\Omega_C t_1}\sin(\pi J_{HH'}\Delta)\cos(\pi J_{HH''}\Delta)\sin(\pi\,{}^nJ_{CH}\Delta)$$
$$+H_-^r H_Z' H_Z'' C_Z e^{i\pi\Omega_C t_1}\sin(\pi J_{HH'}\Delta)\sin(\pi J_{HH''}\Delta)\sin(\pi\,{}^nJ_{CH}\Delta)$$

HMBC:

$$0.5H_-^r C_Z e^{i\pi\Omega_C t_1}\cos(\pi J_{HH'}\Delta)\cos(\pi J_{HH''}\Delta)\sin(\pi\,{}^nJ_{CH}\Delta)$$
$$+iH_-^r C_Z H_Z' e^{i\pi\Omega_C t_1}\cos(\pi J_{HH'}\Delta)\sin(\pi J_{HH''}\Delta)\sin(\pi\,{}^nJ_{CH}\Delta)$$
$$+iH_-^r H_Z'' C_Z e^{i\pi\Omega_C t_1}\sin(\pi J_{HH'}\Delta)\cos(\pi J_{HH''}\Delta)\sin(\pi\,{}^nJ_{CH}\Delta)$$
$$-2H_-^r H_Z' H_Z'' C_Z e^{i\pi\Omega_C t_1}\sin(\pi J_{HH'}\Delta)\sin(\pi J_{HH''}\Delta)\sin(\pi\,{}^nJ_{CH}\Delta)$$

The consequences of the different behavior of the LR-HSQC and HMBC experiment respectively may be visualized by simulation (Figure S6). Again and similar to the outcome for a H^{r}H'C three-spin system the $J_{HH'}$ and Δ dependent intensity variations of the four terms compensate each other in the HMBC, but only partially in the LR-HSQC experiment.

Analysis of n-spin systems

The product operator analysis for an *n*-spin system becomes very lengthy, but some general features can still be derived. For a five spin system, operators like *2H^r_XC$_Z$*, *4H^r_YH'$_Z$C$_Z$*, *4H^r_YH''$_Z$C$_Z$*, *8H^r_XH'$_Z$H''$_Z$C$_Z$,* and *16H^r_YH'$_Z$H''$_Z$H'''$_Z$C$_Z$* (8 terms in total) will be present and will contribute to final signal intensity. Obviously, the lineshapes are rather complicate to be described, because of the overlap of both several absorption and dispersion components. However, most importantly, and corroborated by simulation (Figure S7) for a model CH^{r}H'H''H''' spin system, the zero-crossing points for the signal intensity *always* and *exclusively* occur when the long-range coupling evolution delay Δ matches the inverse of the heteronuclear coupling constant $^nJ_{CH}$, irrespective of the value of *all* homonuclear coupling constants $J_{HH'}$, $J_{HH'}$ *and* $J_{HH'''}$.

This article is protected by copyright. All rights reserved.

Experimental Results

Ethylbenzene

In Figure 5, sections of 2D HMBC and LR-HSQC spectra of 0.1% ethylbenzene dissolved in $CDCl_3$ showing long-range correlations associated with the CH_2 and CH_3 resonances are presented. With the initial delay Δ adjusted to 65.8 ms, and with the value of the homonuclear coupling constant $^3J_{CH2CH3}$ = 7.6 Hz the condition $\Delta = 0.5/^3J_{CH2CH3}$ is fulfilled for which the intensity differences between LR-HSQC and HMBC are expected to be most pronounced. All long-range correlation cross-peaks are expected to be weak in the LR-HSQC- compared to the HMBC-spectrum irrespective of the value of the long-range proton-carbon coupling constant $^nJ_{CH}$, which is experimentally corroborated (Figure 5).

On the other hand, as expected, the HMBC and LR-HSQC spectra recorded with Δ adjusted to a long-range coupling constant of 5 Hz exhibit less differences, but the correlations are still more intense in the HMBC spectrum (Figure S8).

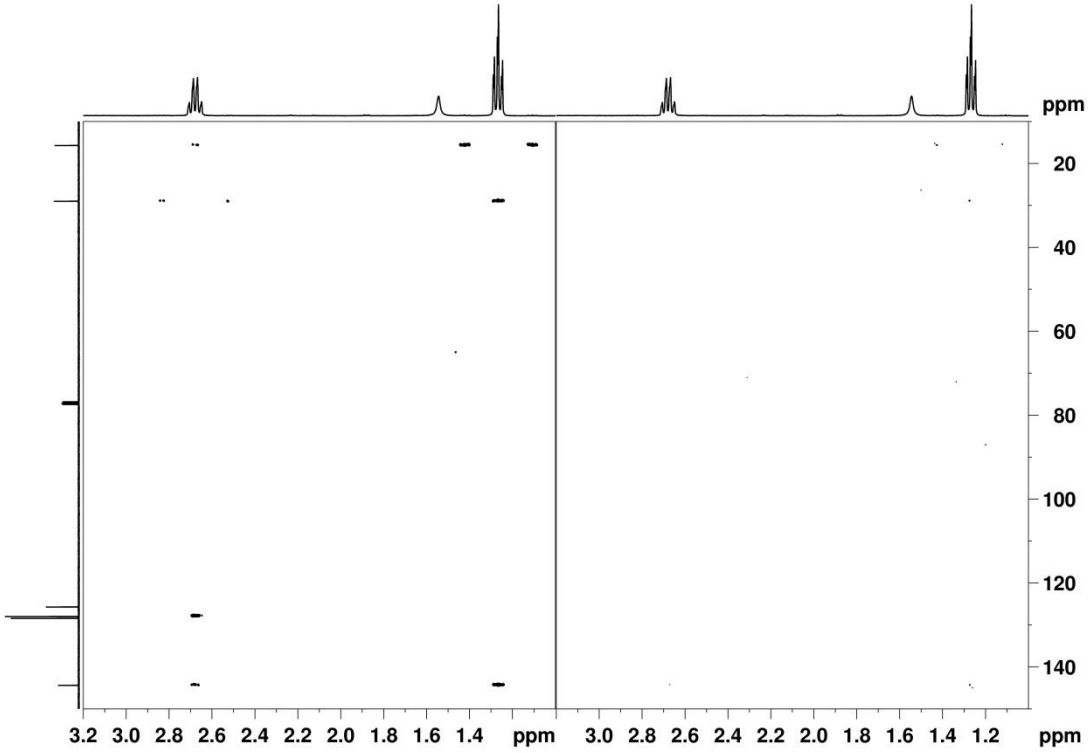

This article is protected by copyright. All rights reserved.

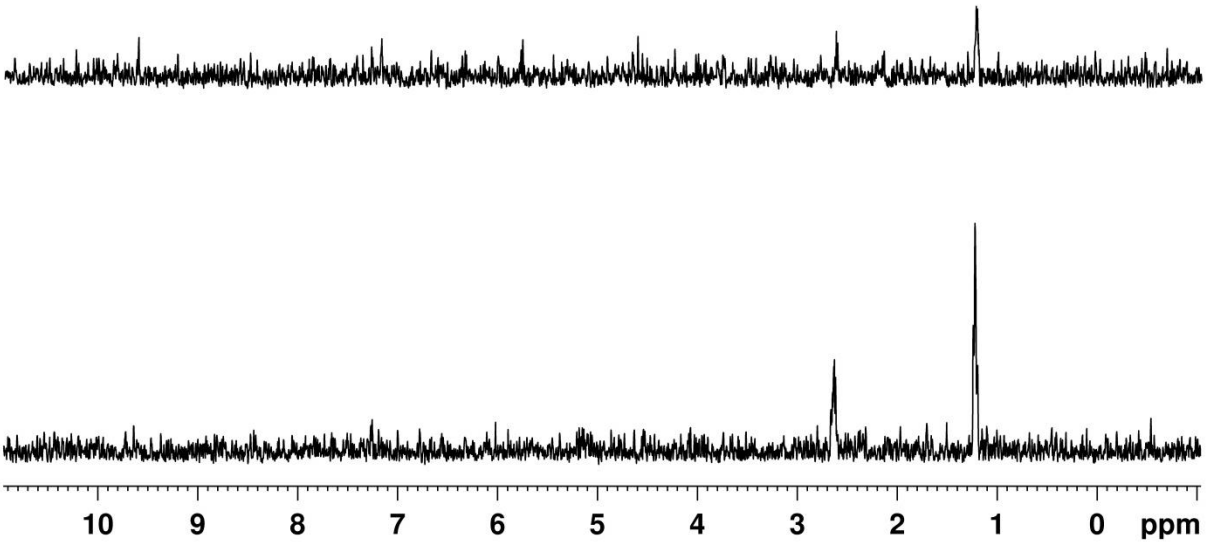

Figure 5. Top: Segments of the 7.6 Hz (that exactly matches the homonuclear $^{3}J_{CH2CH3}$ coupling constant between the CH_2 and the CH_3 protons) adjusted HMBC (left) and LR-HSQC (right) spectra of 0.1% ethylbenzene dissolved in $CDCl_3$ showing $^{n}J_{CH}$ long-range correlations associated with the CH_2 and CH_3 resonances. Both spectra are displayed at the same noise level. Bottom: 1D rows extracted from the HMBC (bottom) and LR-HSQC (top) showing the $^{n}J_{CH}$ long-range correlations associated with the C_{ipso} resonance (δ = 144.3 ppm). Both 1D spectra are displayed at the same noise level.

Strychnine

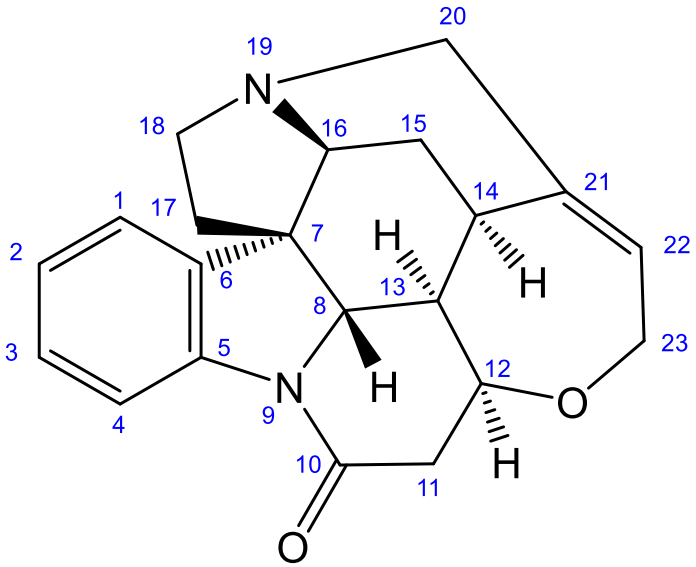

Accepted Article

This article is protected by copyright. All rights reserved.

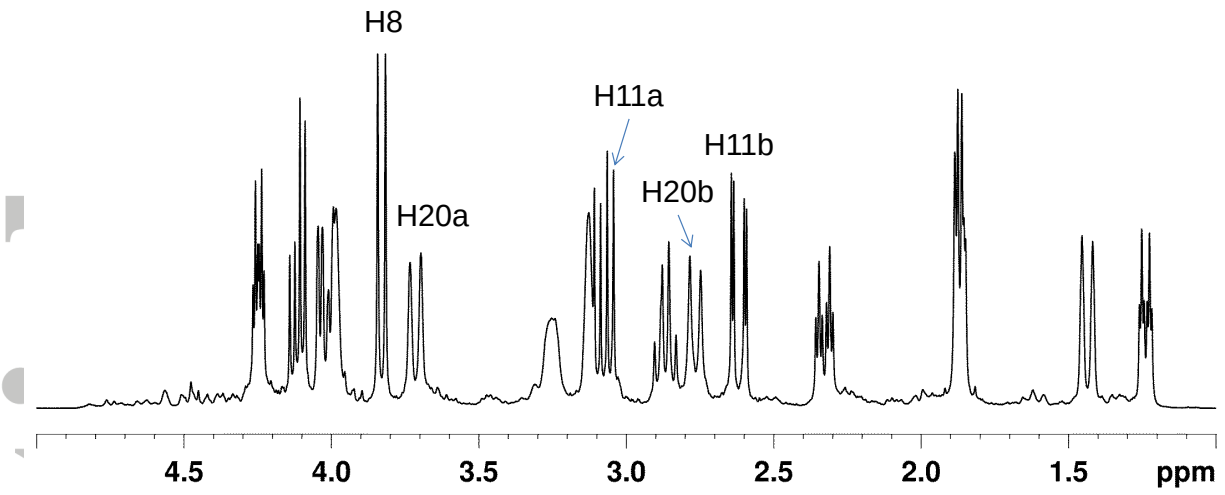

Figure 6. Chemical structure of strychnine (top) and segment of the ^{1}H NMR spectrum of 20 mg strychnine dissolved in 600 µL of deuterochloroform in a 5 mm NMR tube recorded at an observation frequency of 400 MHz. The spectrum was recorded in 8 transients digitized with 64K data points.

The resonances of H8 ($^{3}J_{H8H13}$ = 10.5 Hz), and of H20a and H20b ($^{2}J_{H20aH20b}$ = 14.9 Hz) of strychnine (Figure 6) exemplify the case of CH^{r}H' spin systems, while the resonances of H11a and H11b illustrate the case of CH^{r}H'H'' spin systems ($^{2}J_{H11aH11b}$ = 17.5 Hz, $^{3}J_{H11aH12}$ = 8.4 Hz, $^{3}J_{H11bH12}$ = 3.2 Hz) (Figure 6). Series of 1D ^{13}C-selective HMBC and LR-HSQC spectra centered on the resonance of H8 (δ = 3.83 ppm) and with the selective ^{13}C-pulse adjusted to the resonance of C12 (δ = 77.5 ppm) are shown as a function of the long-range evolution delay Δ (Figure 7 & 8). Other examples are shown in the Supplementary information (Figures S9 & S10).

Accepted Article

This article is protected by copyright. All rights reserved.

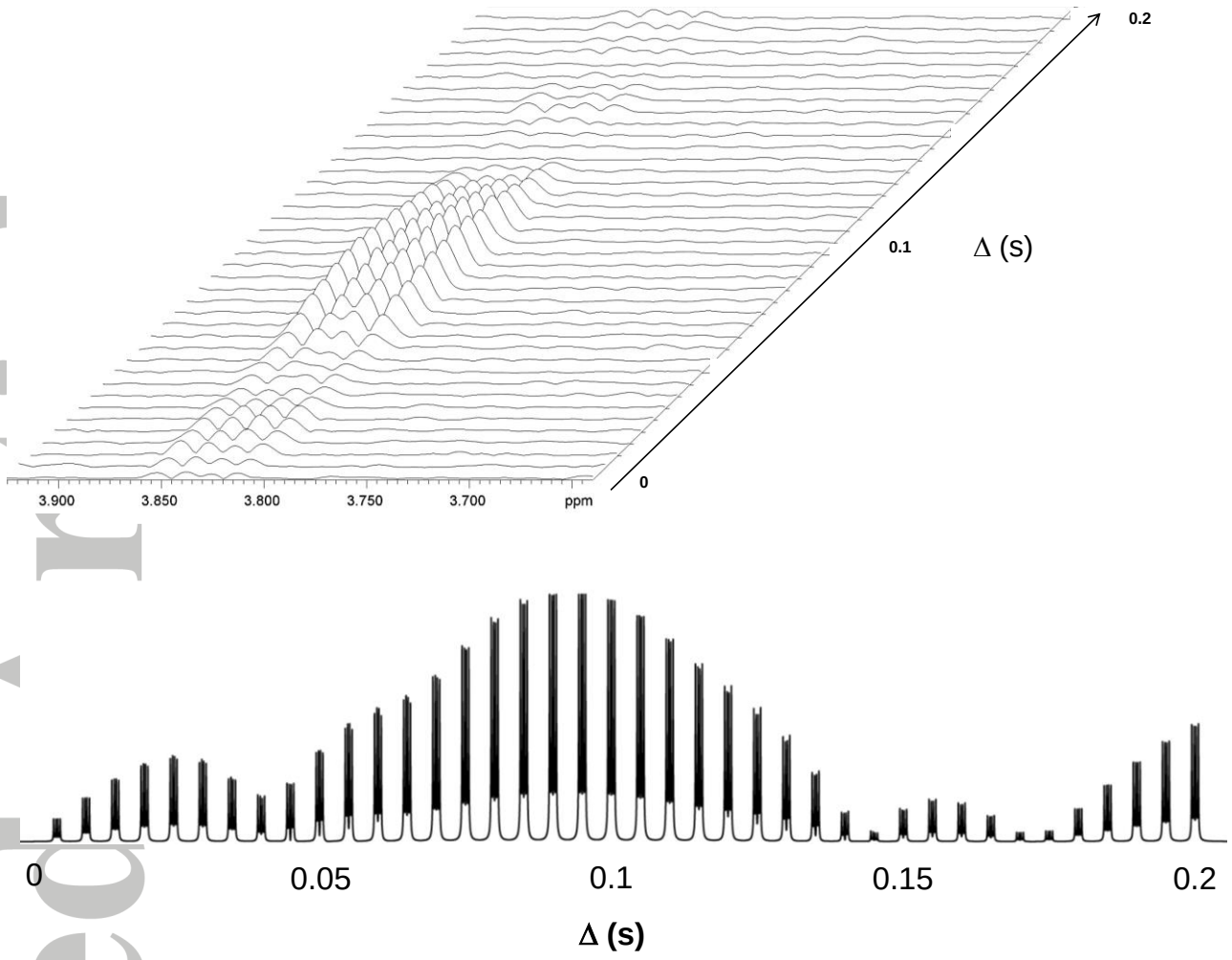

Figure 7. Top: Series of 40 1D ^{13}C-selective LR-HSQC spectra, obtained using a 1D selective version of the pulse sequence shown in Figure 1, as a function of the long-range evolution delay Δ. The resonance of C12 (δ = 77.5 ppm) was selected using a 2 ms Gaussian pulse. The spectra show the resonance of H8 (δ = 3.83 ppm). The spectra are displayed in magnitude mode. Bottom: Simulated spectra obtained for the $C_{12}H_8H_{13}$ spin system. The spectra are displayed in magnitude mode. Parameters used for the simulations: $^3J_{C12H8}$ = 5.8 Hz, $^3J_{H12H13}$ = 10.5 Hz. The relaxation times for H8 have been set to T_1 = 1 s, T_2 = 0.3 s, and relaxation during both the sequence and acquisition was taken into account. Simulations have been performed with the BRUKER NMRSIM program for WINDOWS (version 5.5.3. 2012).

For the LR-HSQC spectra, it can be seen that simulated and experimental spectra correspond to each other and that especially the intensity drops (at Δ = 45, 145, and 170 ms) match very well (Figure 7).

This article is protected by copyright. All rights reserved.

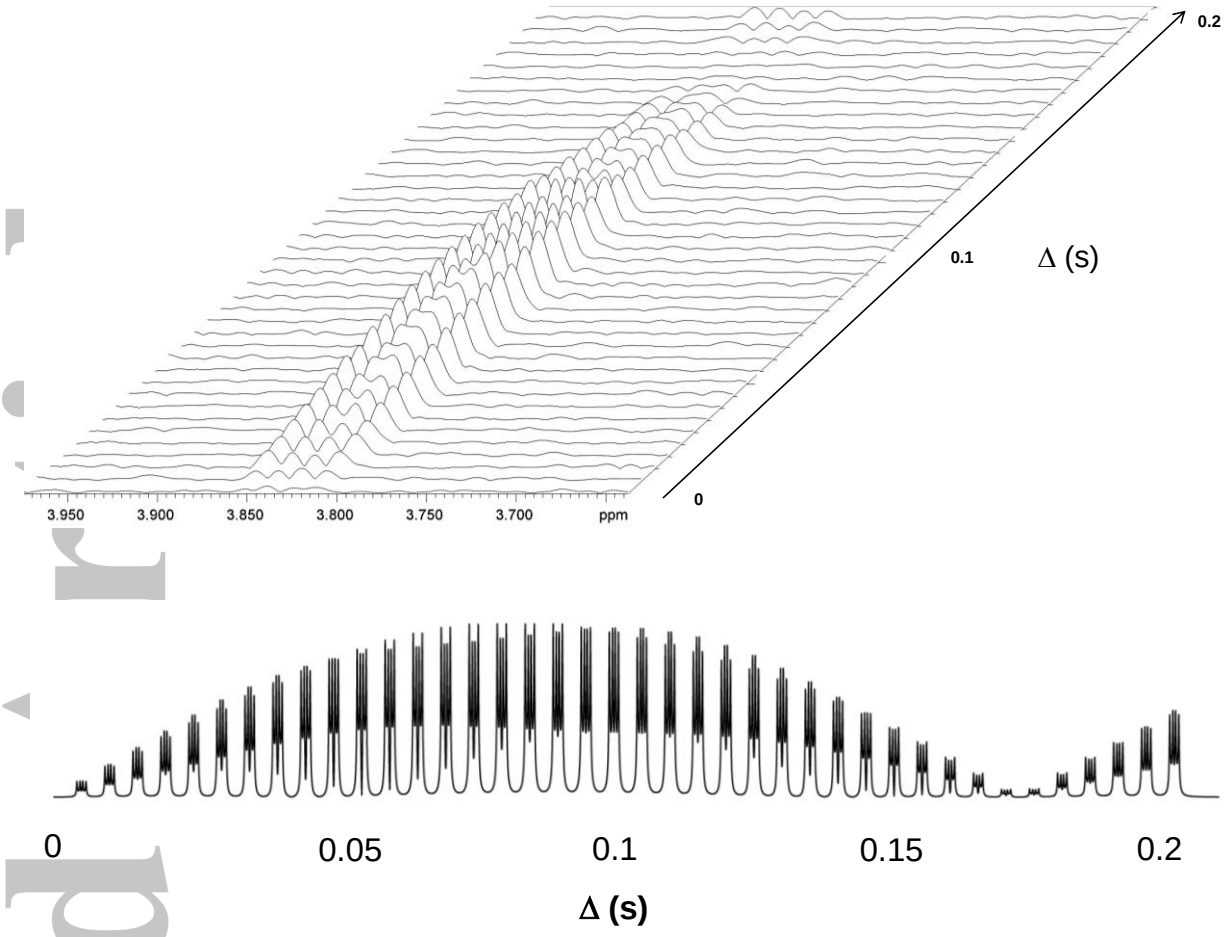

Figure 8. Top: Series of stacked 1D selective HMBC spectra, obtained using a 1D ^{13}C-selective version of the pulse sequence shown in Figure 3, as a function of the long-range evolution delay Δ. The resonance of C12 (δ = 77.5 ppm) was selected using a 2 ms Gaussian pulse. The spectra show the resonance of H8 (δ = 3.83 ppm). The spectra are displayed in magnitude mode. Bottom: Simulated spectra obtained for the $C_{12}H_8H_{13}$ spin system. The spectra are displayed in magnitude mode. Parameters used for the simulations: $^3J_{C12H8}$ = 5.8 Hz, $^3J_{H8H13}$ = 10.5 Hz. The relaxation times for H8 and H13 have been set to T_1 = 1 s, T_2 = 0.5 s (see Supporting Information), and relaxation during both the sequence and acquisition was taken into account. Simulations have been performed with the BRUKER NMRSIM program for WINDOWS (version 5.5.3. 2012).

In line with the results of the product operator treatment shown before the unique zero in both the experimental and simulated spectra for HMBC (Figure 8) occurs for Δ ~ 0.17 s, which corresponds to a long-range coupling constant of ~ 5.8 Hz and matches the condition $\Delta = 1/^3J_{C12H8}$. It turns out that 1D ^{13}C-selective HMBC experiments can used for accurately measuring long-range coupling constants of

This article is protected by copyright. All rights reserved.

any size. The 1D experiment is most advantageously if only a few $^{n}J_{CH}$ values for structural elucidation,[49, 50] have to be determined, as described and demonstrated elsewhere.[34, 51]

Parts of HMBC and LR-HSQC spectra of strychnine with two selected cross-peaks of carbons C21 and C6, respectively, recorded for different long-range evolution delays Δ are shown in Figure 9. The heteronuclear $^{3}J_{C21H13}$ (J = 7.4-7.8 Hz)[52-55] and $^{3}J_{C6H17}$ (J = 1.8-1.9 Hz)[53] cross peaks are indicated with arrows and highlighted with blue and green boxes, respectively. These two cross peaks illustrate the general case of protons coupled to several other protons, which, in the case of the LR-HSQC experiment, is expected to significantly modulate the cross peak's intensity as a function of the long-range evolution delay Δ. Clearly, the $^{3}J_{C6H17}$ cross peak (blue boxes) is visible in all five HMBC spectra, with approximately equal intensity. In contrast, this cross peak is very weak in the LR-HSQC spectrum recorded with Δ = 29 ms and weak for Δ = 48 ms. Likewise, the $^{3}J_{C21H13}$ cross peak (green boxes) is clearly visible in the five HMBC spectra, albeit at a slightly lower intensity for Δ = 29 ms. This cross peak is invisible in the LR-HSQC spectra recorded with Δ = 48 ms and Δ = 59 ms, and remains weak for Δ = 29, 71, and 91 ms. In Figure S11, 1D rows extracted from both experiments recorded with Δ = 71 ms exhibiting the long range correlations of C12 at a chemical shift of 77.5 ppm are shown. Clearly, all long-range correlations appear significantly more intense using the HMBC experiment. The average SNR observed for these two cross-peaks in both HMBC and LR-HSQC spectra shown in Fig. 9 is given in the supplementary material (Table 1).

Accepted Article

This article is protected by copyright. All rights reserved.

Accepted Article

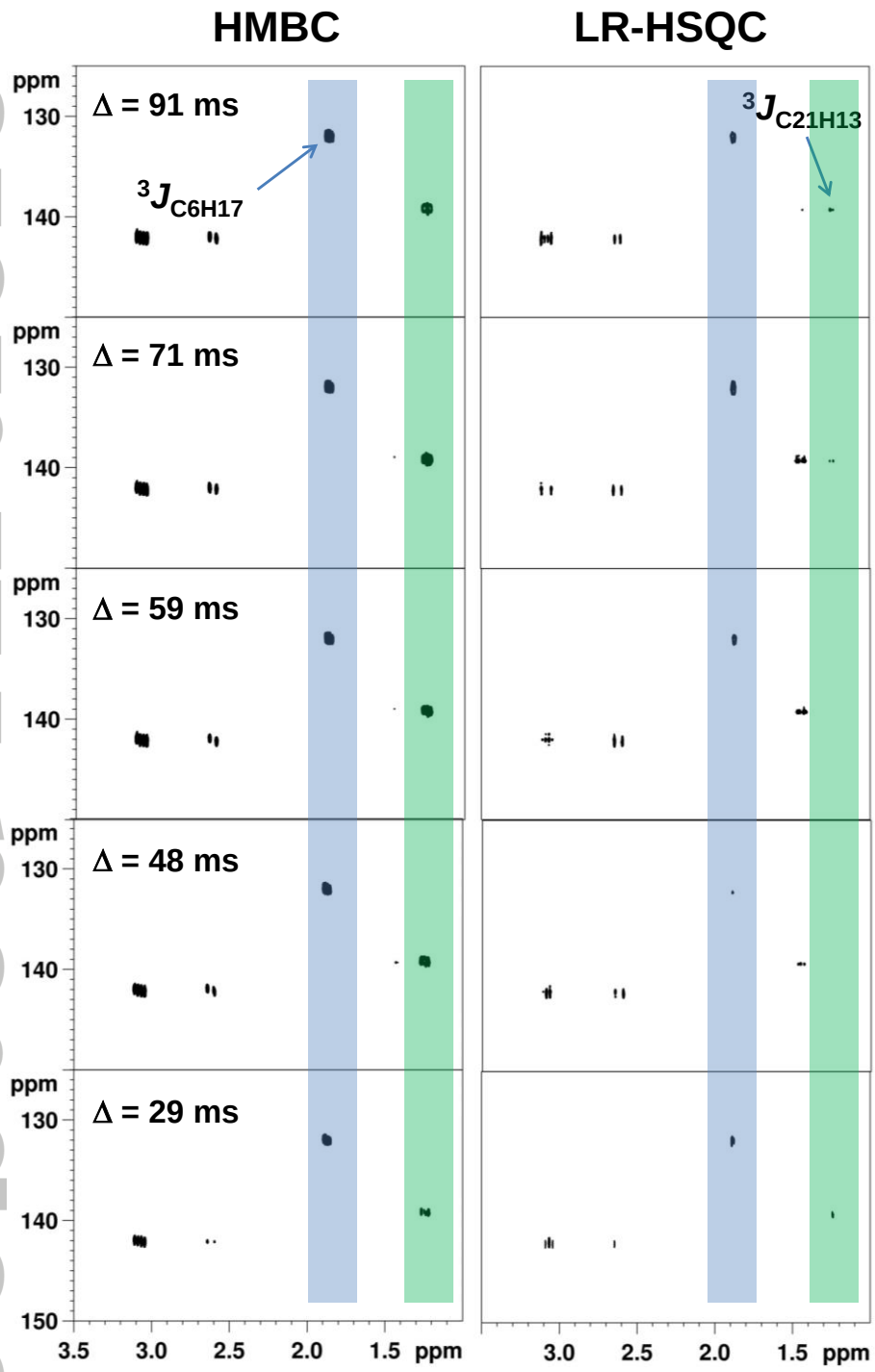

Figure 9. Parts of the HMBC spectra (left), and LR-HSQC spectra (right) of strychnine recorded for different long-range evolution delays Δ. The $^3J_{C21H13}$ and $^3J_{C6H17}$ cross peaks are indicated with arrows and highlighted with blue and green boxes, respectively. All spectra are displayed in magnitude mode and at the same noise level.

This article is protected by copyright. All rights reserved.

LR-HSQC and HMBC-SE experiments are typically acquired and processed in phase sensitive mode. Using this presentation, the LR-HSQC delivers better resolution in F1 compared to the standard HMBC-SE experiment (Figure S12), provided sufficient t_1 increments are recorded. In practice, for the same experiment time, it's therefore conceivable to perform more scans and acquire fewer increments in F1 with the LR-HSQC to deliver the equivalent resolution that one would expect with the standard HMBC data set using fewer scans and more increments. A simple way to avoid the broadening in F1 for the HMBC is to use the CT-HMBC experiments, which provide cross peaks with a resolution similar to that achieved using the LR-HSQC experiment.[23] Also presented in phase sensitive mode, the standard HMBC-SE is more sensitive than the LR-HSQC experiment (Figure S13).

Conclusion

It is commonly claimed that the evolution of the homonuclear proton-proton $J_{HH'}$ couplings during the initial delay Δ of LR-HSQC and HMBC pulse sequences contributes a $\Sigma_i \cos(\pi J_{HHi}\Delta)$ trigonometric factor to the intensity of the observed magnetization, which might cause accidental cancellation of cross-peaks in the spectra.

We have shown with our investigation that this still widespread belief is not fully correct. For both experiments, we have demonstrated both theoretically and experimentally that long-range correlation peaks will *not* be canceled because of homonuclear couplings $J_{HH'}$ but may be weakened at most (LR-HSQC). For a CH^rH' spin system, *two* coherences contribute to the final signal in both experiments: $H^r\text{-}C_Z$ and $H^r\text{-}H'_ZC_Z$. The different behavior of LR-HSQC and HMBC with respect to homonuclear couplings can be attributed to the following: For LR-HSQC and for a CH^rH' three spin system the finally detected $H^r\text{-}H'_ZC_Z$ originates only from one of the components (the single quantum component) of the intermediate coherence $4H^r_YH'_XC_Y$ that survives after the INEPT transfer, while for HMBC the intermediate multiple quantum coherence $4H^r_YH'_ZC_Y$ present after the polarization transfer period is *entirely* converted back into observable $H^r\text{-}H'_ZC_Z$ coherence before acquisition. As

This article is protected by copyright. All rights reserved.

a result, the HMBC experiment is inherently more sensitive compared to the LR-HSQC experiment. This is attributed to the fact that for the HMBC– but not for the LR-HSQC-) experiment the $J_{HH'}$ and Δ dependent intensity variations of the two coherences which contribute to the final signal, $H^r\text{-}C_Z$, containing a $\cos(\pi^n J_{HH'}\Delta)$ term and $H^r\text{-}H'_Z C_Z$ containing a $\sin(\pi^n J_{HH'}\Delta)$ term compensate each other when Δ is varied. This outcome can be generalized to *n*-spin systems as demonstrated for a $CH^rH'H''$ spin system.

In both experiments, the cross peak's intensity always and exclusively vanishes for the condition $\Delta = k/^nJ_{CH}$, irrespective of the magnitude and numbers of additional passive homonuclear $^nJ_{HH'}$ couplings. However, for the LR-HSQC experiment, homonuclear couplings $J_{HH'}$ cause severe drops of the long-range correlation's intensity at certain $^nJ_{HH'}$ dependent values of Δ, while the cross peak's intensity in HMBC spectra follows a simple $\sin(\pi^n J_{CH}\Delta)\exp(-\Delta/T_{2eff})$ dependence.

HMBC-based experiments are therefore the best choice among the family of heteronuclear long-range correlation experiments because: (i) the overall cross peak's intensity is generally higher, and (ii) in LR-HSQC experiments the intensity of the long-range cross peaks is additionally influenced in an unwanted way by the magnitude and number of passive homonuclear proton-proton couplings $J_{HH'}$. Therefore, depending on the choice of the long-range coupling delay Δ, important correlations might be missing with LR-HSQC.

Experimentally, it turned out that a refocused HSQC experiment optimized for long-range couplings, the LR-HSQMBC experiment, performs much better than the D-HMBC, not only for very long-range responses, but also for the total number of $^nJ_{CH}$ correlations.[17] For strychnine, the LR-HSQMBC provided a total of 68 very long-range correlations that reached further than 3 bonds ($>^3J_{CH}$). There were 14 more very long-range responses compared with the 2 Hz HMBC, and 24 more very long-range responses than were observed in the D-HMBC data. The LR-HSQMBC also revealed a total of 160 $^nJ_{CH}$ correlations, while 142 correlations were observed using the 2 Hz HMBC, and only 115 correlations in the D-HMBC data. Here, it should be mentioned that many of the very long-range correlations that can be observed in an LR-HSQMBC spectrum may not be observed at all when less than 512 t_1 increments are acquired in the F1 dimension. In many instances, $^5J_{CH}$ and $^6J_{CH}$ correlations aren't observed until 640 or even 768 t_1 increments have been

This article is protected by copyright. All rights reserved.

acquired.[17, 56] We are currently investigating theoretically and experimentally both experiments to explore these experimental evidences.

References

[1] E. Kupce, R. Freeman, *Magn. Reson. Chem.* **2010**, *48*, 333-336.

[2] A. V. Buevich, R. T. Williamson, G. E. Martin, *J. Nat. Prod.* **2014**, *77*, 1942-1947.

[3] L. Castanar, J. Sauri, R. T. Williamson, A. Virgili, T. Parella, *Angew. Chem., Int. Ed. Engl.* **2014**, *53*, 8379-8382.

[4] R. T. Williamson, A. V. Buevich, G. E. Martin, *Tetrahedron Lett.* **2014**, *55*, 3365-3366.

[5] L. Castanar, T. Parella, in *Annu. Rep. NMR Spectrosc., Vol. 84* (Ed.: G. A. Webb), **2015**, pp. 163-232.

[6] M. Elyashberg, *Trac-Trends in Analytical Chemistry* **2015**, *69*, 88-97.

[7] J. Sauri, M. Frederich, A. T. Tchinda, T. Parella, R. T. Williamson, G. E. Martin, *J. Nat. Prod.* **2015**, *78*, 2236-2241.

[8] J. Sauri, G. E. Martin, J. Furrer, *Concepts Magn. Reson., Part A* **2015**, *44A*, 227-251.

[9] J. Sauri, Y. Z. Liu, T. Parella, R. T. Williamson, G. E. Martin, *J. Nat. Prod.* **2016**, *79*, 1400-1406.

[10] G. E. Martin, A. S. Zektzer, *Magn. Reson. Chem.* **1988**, *26*, 631-652.

[11] G. E. Martin, R. C. Crouch, *J. Nat. Prod.* **1991**, *54*, 1-70.

[12] G. E. Martin, C. E. Hadden, *J. Nat. Prod.* **2000**, *63*, 543-585.

[13] A. M. Torres, W. A. Bubb, P. W. Kuchel, *J. Magn. Reson.* **2002**, *156*, 249-257.

[14] A. Bax, M. F. Summers, *J. Am. Chem. Soc.* **1986**, *108*, 2093-2094.

[15] J. Furrer, *Concepts Magn. Reson., Part A* **2012**, *40A*, 101-127.

[16] J. Furrer, *Concepts Magn. Reson., Part A* **2012**, *40A*, 146-169.

[17] R. T. Williamson, A. V. Buevich, G. E. Martin, T. Parella, *J. Org. Chem.* **2014**, *79*, 3887-3894.

[18] K. Furihata, H. Seto, *Tetrahedron Lett.* **1995**, *36*, 2817-2820.

[19] R. Wagner, S. Berger, *Magn. Reson. Chem.* **1998**, *36*, S44-S47.

This article is protected by copyright. All rights reserved.

[20] C. E. Hadden, G. E. Martin, V. V. Krishnamurthy, *J. Magn. Reson.* **1999**, *140*, 274-279.

[21] G. E. Martin, C. E. Hadden, R. C. Crouch, V. V. Krishnamurthy, *Magn. Reson. Chem.* **1999**, *37*, 517-523.

[22] C. E. Hadden, G. E. Martin, V. V. Krishnamurthy, *Magn. Reson. Chem.* **2000**, *38*, 143-147.

[23] K. Furihata, H. Seto, *Tetrahedron Lett.* **1998**, *39*, 7337-7340.

[24] T. D. W. Claridge, I. Perez-Victoria, *Org. Biomol. Chem.* **2003**, *1*, 3632-3634.

[25] L. Kay, P. Keifer, T. Saarinen, *J. Am. Chem. Soc.* **1992**, *114*, 10663-10665.

[26] D. O. Cicero, G. Barbato, R. Bazzo, *J. Magn. Reson.* **2001**, *148*, 209-213.

[27] A. Meissner, O. W. Sorensen, *Magn. Reson. Chem.* **2001**, *39*, 49-52.

[28] H. Kogler, O. W. Sørensen, G. Bodenhausen, R. R. Ernst, *J. Magn. Reson.* **1983**, *55*, 157-163.

[29] E. Kupče, R. Freeman, *Magn. Reson. Chem.* **2007**, *45*, 2-4.

[30] J. Furrer, *Chem. Commun. (Cambridge, U. K.)* **2010**, *46*, 3396-3398.

[31] J. Furrer, in *Annu. Rep. NMR Spectrosc., Vol. 74* (Ed.: G. A. Webb), Academic Press, **2011**, pp. 293-354.

[32] W. Schoefberger, J. Schlagnitweit, N. Müller, in *Annu. Rep. NMR Spectrosc., Vol. 72* (Ed.: G. A. Webb), Academic Press, **2011**, pp. 1-60.

[33] J. Furrer, *Concepts Magn. Reson., Part A* **2015**, *43*, 177-206.

[34] P. Bigler, J. Furrer, *Magn. Reson. Chem.* **2018**, *56*, 329-337.

[35] G. Bodenhausen, D. Ruben, *Chem. Phys. Lett.* **1980**, *69*, 185-189.

[36] R. Marek, L. Kralik, V. Sklenar, *Tetrahedron Lett.* **1997**, *38*, 665-668.

[37] R. T. Williamson, B. L. Marquez, W. H. Gerwick, K. E. Kover, *Magn. Reson. Chem.* **2000**, *38*, 265-273.

[38] W. R. Croasmun, R. M. K. Carlson, *Two-dimensional NMR spectroscopy. Applications for chemists and biochemists*, VCH Publishers,New York, NY, **1987**.

[39] H. Koskela, I. Kilpeläinen, S. Heikkinen, *J. Magn. Reson.* **2003**, *164*, 228-232.

[40] R. E. Hurd, B. K. John, *J. Magn. Reson.* **1991**, *91*, 648-653.

[41] J. Keeler, *Understanding NMR Spectroscopy*, Wiley, **2011**.

[42] R. R. Ernst, G. Bodenhausen, A. Wokaun, *Principles of nuclear magnetic resonance in one and two dimensions*, Clarendon Press, Oxford, **1987**.

[43] G. Wider, K. Wuthrich, *J. Magn. Reson. B* **1993**, *102*, 239-241.

This article is protected by copyright. All rights reserved.

Accepted Article

[44] T. E. Burrow, R. G. Enriquez, W. F. Reynolds, *Magn. Reson. Chem.* **2009**, *47*, 1086-1094.

[45] F. A. A. Mulder, C. A. E. M. Spronk, M. Slijper, R. Kaptein, R. Boelens, *J. Biomol. NMR* **1996**, *8*, 223-228.

[46] K. E. Kover, G. Batta, K. Feher, *J. Magn. Reson.* **2006**, *181*, 89-97.

[47] H. Koskela, I. Kilpeläinen, S. Heikkinen, *J. Magn. Reson.* **2016**, *272*, 114-122.

[48] R. R. Ernst, G. Bodenhausen, A. Wokaun, in *Principles of nuclear magnetic resonance in one and two dimensions*, Clarendon Press, Oxford, **1987**, p. 504.

[49] N. Nath, Lokesh, N. Suryaprakash, *ChemPhysChem* **2012**, *13*, 645-660.

[50] T. Parella, J. F. Espinosa, *Prog. Nucl. Magn. Reson. Spectrosc.* **2013**, *73*, 17-55.

[51] W. Willker, D. Leibfritz, *Magn. Reson. Chem.* **1995**, *33*, 632-638.

[52] V. V. Krishnamurthy, *J. Magn. Reson.* **1996**, *121*, 33-41.

[53] R. A. E. Edden, J. Keeler, *J. Magn. Reson.* **2004**, *166*, 53-68.

[54] C. P. Butts, B. Heise, G. Tatolo, *Org. Lett.* **2012**, *14*, 3256-3259.

[55] C. Hoeck, C. H. Gotfredsen, O. W. Sorensen, *J. Magn. Reson.* **2017**, *275*, 68-72.

[56] G. E. Martin, *private communication* **2018**.

Accepted Article

This article is protected by copyright. All rights reserved.

Why is HMBC superior to LR-HSQC? Influence of homonuclear couplings $J_{HH'}$ on the intensity of long-range correlations

Peter Bigler*, Julien Furrer*

HMBC or LR-HSQC? HMBC is superior to LR-HSQC for detecting long-range heteronuclear correlations, because: (i) the cross peak's intensity is higher, and (ii) in LR-HSQC the intensity of the cross peaks is additionally influenced in an unwanted way by the magnitude and number of passive homonuclear proton-proton couplings $J_{HH'}$. Notably, for both experiments, long-range correlations *do not* cancel because of homonuclear couplings $J_{HH'}$.

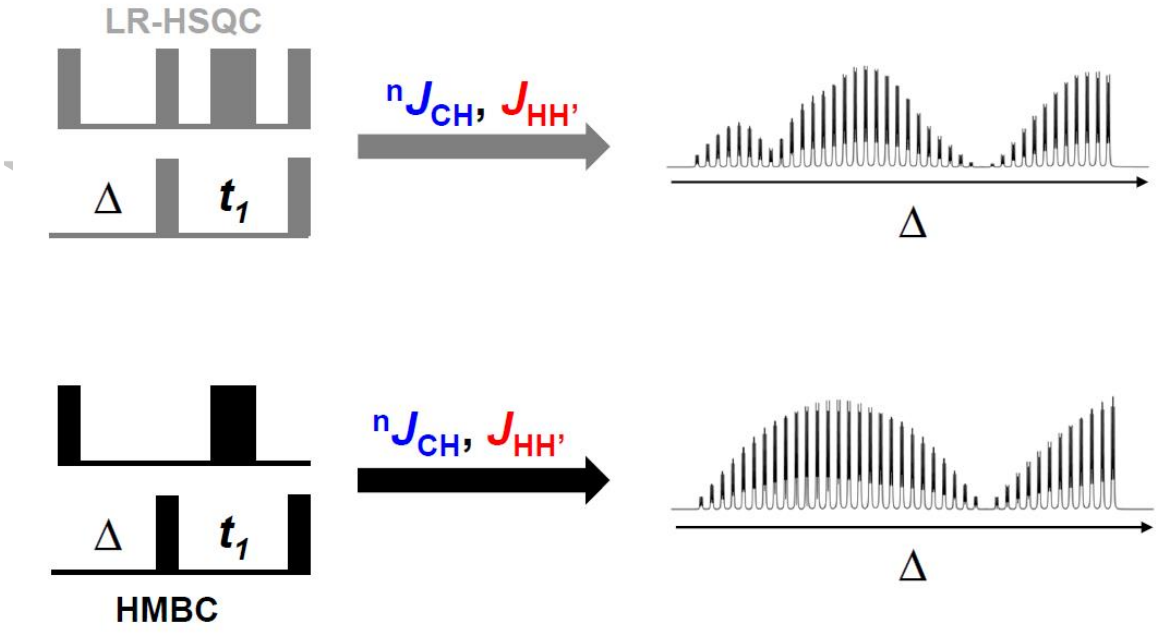

This article is protected by copyright. All rights reserved.